A Finite-Volume method for compressible non-equilibrium two-phase flows in networks of elastic pipelines using the Baer–Nunziato model

Frédéric Daude, R.A. Berry, P. Galon

A Finite-Volume method for compressible non-equilibrium two-phase flows in networks of elastic pipelines using the Baer-Nunziato model

F. Daude[a,b], R. A. Berry[c], P. Galon[a,d]

[a] *IMSIA, UMR EDF-CNRS-CEA-ENSTA 9219, Université Paris-Saclay, F-91762 Palaiseau, France*
[b] *EDF R&D, ERMES, F-91120 Palaiseau, France*
[c] *Idaho National Laboratory, P.O. Box 1625 Idaho Falls, ID 83415, USA*
[d] *CEA Saclay, DEN/SEMT, Université Paris-Saclay, F-91191 Gif-sur-Yvette, France*

Abstract

A novel Finite-Volume scheme for the numerical computations of compressible two-phase flows in pipelines is proposed for the fully non-equilibrium Baer-Nunziato model. The present FV approach is the extension of the method proposed in [1] in the context of the Euler equations to the Baer-Nunziato model. In addition, proper approximations of the non-conservative terms are proposed to consider jumps of volume fraction as well as jumps of cross-section in order to respect uniform pressure and velocity profiles preservation. In particular, focus is given to the numerical treatment of abrupt changes in area and to networks wherein several pipelines are connected at junctions. The proposed method makes it possible to avoid the use of an iterative procedure for the solution of the junction problem. The present approach can also deal with general Equations Of State. In addition, the fluid-structure interaction of compressible fluid flowing in flexible pipes is also considered. The proposed scheme is then assessed on a variety of shock-tubes and other transient flow problems and experiments demonstrating its capability to resolve such problems efficiently, accurately and robustly.

Keywords: Variable cross-section (temporal and spatial), Baer-Nunziato model, Finite Volume, ALE formulation, Pipe network, Junction of flexible pipes

1. Introduction

One-dimensional unsteady or transient compressible flow computations in ducts with variable cross-section are of interest in many industrial and engineering applications involving complex pipe systems. Many papers dealing with variable cross-section pipelines encountered in the literature consider the Euler equations [2, 3, 4, 5]. Much less is known about compressible multiphase flows. In particular, Berry *et al.* [6] have proposed one of the first approaches dealing with variable cross-sections with Baer-Nunziato-type models. These papers often only consider one single pipe and not networks composed by a complex pipeline system connected by junctions. Many different approaches are proposed in the literature to solve this problem. In most of the methods, the coupling conditions are based on the mass conservation at the junction. In addition, some of them assume that all the pipes should be at the same pressure at the junction [7, 8, 9] or the same total pressure at the junction [10]. Other authors treat the junction coupling as a generalized Riemann problem [11, 12, 13, 14] or so called "half Riemann" problem [10]. However, only isentropic or isothermal Euler equations are considered in most of these papers. This paper will consider other conditions that should be satisfied in order to couple all of the flow variables. Moreover, most papers encountered in the literature deal with rigid tubes. However, the pipes used in realistic networks are flexible which can affect the internal fluid dynamics. For example, the speed of pressure waves is known to be strongly influenced by the elastic behavior of the pipe [7, 15, 16]. That is why the dynamic behavior of flexible pipes and its interaction with the internal fluid are also considered here. Recently, Dumbser and his co-workers [17, 18, 19] have proposed a finite-volume method for compressible flows in flexible tubes where a path-conservative approach is considered to deal with the spatial

Email address: frederic.daude@edf.fr (F. Daude)

variation of cross-sections. Once again, these papers only consider isentropic or isothermal Euler equations. As the use of path-conservative methods for shock-wave solutions has been well discussed (see for example [20, 21]), this kind of approach is not considered in the present paper. In order to take into account all of the previously mentioned features relevant for the propagation of pressure waves in realistic pipe systems composed by networks of flexible pipes involving potential abrupt change of area, a new Finite-Volume (FV) formulation has been recently proposed [1] for the complete Euler and Homogeneous Equilibrium Model (HEM) equations. This FV approach is based on the integral form of the fluid equations and makes it possible to obtain a discrete 1-D variable cross-section system. It has been shown that general equations of state can be used. In addition, the junction coupling is also tackled using the integral form of the equations in a similar manner as in [22, 23]. As a consequence, no iterative procedure is used for this treatment of the junction problem. This Finite-Volume method was also coupled with a Finite-Element method using the beam theory in [1] for the resolution of fluid-structure interaction between a compressible fluid and the surrounding movable/deformable structure of the tube wall. Furthermore, this FV approach was recently assessed on water-hammer experiments with column-separation [24]. However, only the Homogeneous Equilibrium Model (HEM) was considered for compressible two-phase flows in the previous works [1, 24] as its mathematical structure is essentially the same as the Euler equations for a single-phase flow. The HEM is the simplest two-phase model taking into account phase transitions and is extensively used for the simulation of cavitation, for example [25] and the references herein. Unlike the HEM, the Baer-Nunziato-type (BN) model can represent complex two-phase flow phenomena involving thermodynamical disequilibrium as shown in [26] for the fast depressurization of hot water in pressurized pipes. However, very few works consider variable cross-section in conjunction with the Baer-Nunziato model except the work of Berry and his co-workers [6, 27, 28] in the context of the development of the RELAP-7 code. That is why we here consider the extension of the FV approach proposed [1] in the context of the Euler equations to the two-fluid BN model. This model is considered to be one of the most general full non-equilibrium two-phase flow models. The BN model, which is often built using an averaging procedure of the local conservation laws [29, 30, 31] assumes full non-equilibrium between phases. The mathematical properties of this model without source terms were first studied by Embid and Baer [32]. The main difficulty of the convective part of the model lies in the presence of non-conservative terms. Many numerical approximations based on approximate Riemann solvers have been proposed, see for example [33, 34, 35, 36, 37, 38, 39, 40] and the references herein. To the knowledge of the authors, this is the first time that the Baer-Nunziato model is considered within the use of elastic pipes, abrupt change of area, and junctions of several branches. The main difficulty is to propose numerical approaches able to deal with both the non-conservative terms involved in the change of volume fraction and the non-conservative terms involved in the change of cross-sections. The uniform pressure and velocity preservation becomes a more challenging issue in the context of variable cross-sections.

The paper is organized as follows. Section 2 describes the numerical approximation of the BN model leading to the proposed 1-D discrete FSI model. In particular, the integral form of the Baer-Nunziato equations is carefully described showing the numerical approximations of both volume fraction and cross-section gradients. In addition, the numerical approach proposed for both the junction problem and the abrupt change of area is clearly detailed. The present numerical method is then assessed on several transient problems in Section 3. Especially, the interaction of shock waves in both gas and liquid with a sudden change of area, the pressure wave propagation in rigid and elastic pipes, a water-hammer experiment with vapor cavity formation and collapse, and finally the propagation of pressure waves in a network are satisfactorily demonstrated.

2. Governing equations and numerical procedure

2.1. Baer-Nunziato two-phase model

2.1.1. Governing equations

The unsteady compressible multi-dimensional two-pressure two-fluid equations (without source terms) are given by:

$$\partial_t \boldsymbol{U} + \nabla \cdot \boldsymbol{F}(\boldsymbol{U}) + \boldsymbol{H}(\boldsymbol{U}) \nabla \alpha_1 = \boldsymbol{0} \tag{1}$$

with

$$\boldsymbol{U} = \begin{pmatrix} \alpha_1 \\ \alpha_k\rho_k \\ \alpha_k\rho_k\boldsymbol{u}_k \\ \alpha_k\rho_k e_k \end{pmatrix}, \quad \boldsymbol{F}(\boldsymbol{U}) = \begin{pmatrix} \boldsymbol{0} \\ \alpha_k\rho_k\boldsymbol{u}_k \\ \alpha_k\rho_k\boldsymbol{u}_k\otimes\boldsymbol{u}_k + \alpha_k p_k \boldsymbol{I_d} \\ \alpha_k\left(\rho_k e_k + p_k\right)\boldsymbol{u}_k \end{pmatrix} \quad \text{and} \quad \boldsymbol{H}(\boldsymbol{U}) = \begin{pmatrix} \boldsymbol{u}_I \\ \boldsymbol{0} \\ (-1)^k\, p_I \boldsymbol{I_d} \\ (-1)^k\, p_I \boldsymbol{u}_I \end{pmatrix} \quad \text{where} \quad k = 1, 2$$

with the constraint $\alpha_1 + \alpha_2 = 1$. α_k, ρ_k, $\boldsymbol{u}_k$, p_k and e_k denote the volume fraction, density, velocity-vector, pressure and specific total energy of the phase k and $\boldsymbol{I_d}$ is the identity tensor. The specific internal energy of the phase k denoted by ε_k is given by: $\varepsilon_k = e_k - \boldsymbol{u}_k^2/2$. An equation of state (EOS) is considered for each phase gives ε_k as a function of p_k and ρ_k: $\varepsilon_k = \varepsilon_k(p_k, \rho_k)$. The phasic speed of sound c_k is defined as:

$$\rho_k c_k^2 \equiv \left(\frac{p_k}{\rho_k} - \rho_k \partial_{\rho_k}\varepsilon_k\right)\left(\partial_{p_k}\varepsilon_k\right)^{-1}$$

The specific entropy $s_k(p_k, \rho_k)$ satisfies the relation: $c_k^2 \partial_{p_k} s_k + \partial_{\rho_k} s_k = 0$. The temperature T_k of the phase k is defined as: $1/T_k \equiv \partial_{p_k} s_k / \partial_{p_k}\varepsilon_k$. The Baer-Nunziato model [41] is here considered which leads to the following closure laws for the interfacial velocity vector $\boldsymbol{u}_I$ and the interfacial pressure p_I:

$$\boldsymbol{u}_I = \boldsymbol{u}_2 \quad \text{and} \quad p_I = p_1 \tag{2}$$

Note that other choices for $\boldsymbol{u}_I$ and p_I are also encountered in the literature [33, 42, 34]. Some of them are chosen to satisfy an entropy inequality as in [42, 34]. Recent comparisons on these specific entropy-satisfying closure relations have been performed on fast steam-water transients [43] showing that all the considered closure laws provide almost the same grid converged numerical results on those test cases.
The governing equations (1) are hyperbolic (as $|u_I - u_k| \neq c_k$) but not strictly [32]. In 1-D, the seven eigenvalues are:

$$\lambda_1 = u_I, \quad \lambda_2 = u_1 - c_1, \quad \lambda_3 = u_1, \quad \lambda_4 = u_1 + c_1, \quad \lambda_5 = u_2 - c_2, \quad \lambda_6 = u_2 \quad \text{and} \quad \lambda_7 = u_2 + c_2$$

Fields associated with eigenvalues $\lambda_{1,3,6}$ are linearly degenerate (LD), while the other fields are genuinely non-linear (GNL).
Note that the non-conservative term $\boldsymbol{H}(\boldsymbol{U})\nabla\alpha_1$ in Eq. (1) acts only across the contact discontinuity $\boldsymbol{u}_I$, i.e. there is no change of α_1 across the other waves leading to a pair of Euler equations for each phase separately [32, 36]. As a consequence, unique jump conditions can be written within each single phase [42, 34]. In other words, shock solutions of the Riemann problems are defined in an unambiguous way. This is of major importance from a computational point of view: without such properties, numerical grid converged shock solutions may differ due to the inner numerical diffusion of the scheme.
This set of equations is completed by the addition of two phasic equations of state (EOS). In the present paper, the Stiffened Gas (SG) EOS is considered for each phase:

$$\rho_k\varepsilon_k = \frac{p_k + \gamma_k\pi_k}{\gamma_k - 1} + \rho_k q_k \tag{3}$$

where γ_k, π_k and q_k are characteristic constants to render unique the thermodynamic behavior of each fluid.

2.1.2. Integral form of the 3-D equations

The derivation detailed in the following is the extension of the approach proposed in [1] to the Baer-Nunziato model. Focus is thus given to the numerical approximation of the non-conservative terms linked to the change of volume fraction as well as the ones due to the cross-section variations. The starting point of the present method is the integral form of Eq. (1) for a moving control volume $C_i(t)$ as:

$$\frac{\mathrm{d}}{\mathrm{d}t}\left(\int_{C_i(t)} \boldsymbol{U}\mathrm{d}\boldsymbol{V}\right) + \sum_{l\in\partial C_i(t)} \int_l \boldsymbol{F}^{\mathrm{ALE}}(\boldsymbol{U}, \boldsymbol{v})\,\boldsymbol{n}\mathrm{d}\boldsymbol{S} + \int_{C_i(t)} \boldsymbol{H}(\boldsymbol{U})\nabla\alpha_1\mathrm{d}\boldsymbol{V} = \boldsymbol{0} \tag{4}$$

with the ALE (Arbitrary Lagrangian-Eulerian) inviscid conservative flux-vector associated with the BN model and given by:

$$\boldsymbol{F}^{\mathrm{ALE}}(\boldsymbol{U},\boldsymbol{v}) = \begin{pmatrix} -\boldsymbol{v}\alpha_1 \\ \alpha_k\rho_k(\boldsymbol{u}_k-\boldsymbol{v}) \\ \alpha_k\rho_k\boldsymbol{u}_k\otimes(\boldsymbol{u}_k-\boldsymbol{v})+\alpha_k p_k\boldsymbol{I_d} \\ \alpha_k\rho_k e_k(\boldsymbol{u}_k-\boldsymbol{v})+\alpha_k p_k\boldsymbol{u}_k \end{pmatrix}$$

The moving control volume $C_i(t)$ is bounded by the surface $\partial C_i(t)$ on which $\boldsymbol{v}$ and $\boldsymbol{n}$ are the boundary's local velocity and its unit outward normal vector, respectively.

It is well know that, to ensure the conservative properties on moving and/or deforming grids, the geometric conservation law (GCL) has to be satisfied [44]:

$$\frac{\mathrm{d}}{\mathrm{d}t}\Big(|C(t)|\Big) - \int_{\partial C(t)} \boldsymbol{v}\cdot\boldsymbol{n}\mathrm{d}\boldsymbol{S} = 0 \tag{5}$$

This equation is here implicitly satisfied as done previously in [45, 46, 39]. For this purpose, the boundary $\partial C(t)$ is defined as a weighted average of the n and $n+1$ time level areas in the discretization of the BN equations as it will be detailed in the following.

For quasi 1-D geometries such as pipelines, the main flow aligns with the pipe axis so only the axial flow velocity is considered, the second and third velocity components being neglected. For such configurations, the moving control volume $C_i(t)$ is considered to be conical. Its axis, of length h_i corresponds to the flow axis denoted in the following by $\boldsymbol{x}$. The boundary of this volume, $\partial C_i(t)$, is composed of three surfaces: two orthogonal to the pipe (and flow) axis denoted $A_{i\pm1/2}$ and A_w which corresponds to the pipe sidewall as represented in Fig. (1).

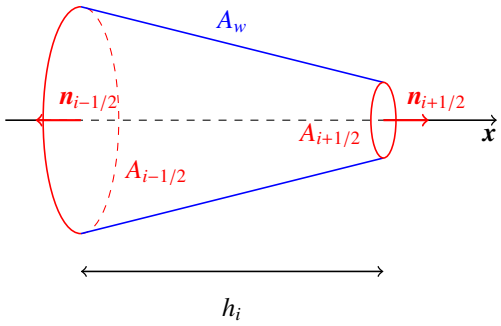

Figure 1: Sketch of the conical control volume C_i of length h_i composed by three surfaces: the two cross-sections $A_{i\pm1/2}$ and the pipe wall A_w.

Separating the conservative terms from the non-conservative ones, the semi-discretization of the integral equation (4) on the cell C_i can be written as:

$$\begin{aligned} \frac{\mathrm{d}}{\mathrm{d}t}(|C_i|\boldsymbol{U}_i) &+ \int_{A_{i+1/2}} \boldsymbol{F}^{\mathrm{ALE}}(\boldsymbol{U},\boldsymbol{v}_{i+1/2})\,\boldsymbol{n}_{i+1/2}\mathrm{d}\boldsymbol{S} &+ \int_{A_{i-1/2}} \boldsymbol{F}^{\mathrm{ALE}}(\boldsymbol{U},\boldsymbol{v}_{i-1/2})\,\boldsymbol{n}_{i-1/2}\mathrm{d}\boldsymbol{S} &+ \int_{A_w} \boldsymbol{F}^{\mathrm{ALE}}(\boldsymbol{U},\boldsymbol{v})\,\boldsymbol{n}\mathrm{d}\boldsymbol{S} \\ &+ \int_{A_{i+1/2}} \boldsymbol{R}_i(\boldsymbol{U})\cdot\boldsymbol{n}_{i+1/2}\mathrm{d}\boldsymbol{S} &+ \int_{A_{i-1/2}} \boldsymbol{R}_i(\boldsymbol{U})\cdot\boldsymbol{n}_{i-1/2}\mathrm{d}\boldsymbol{S} &+ \int_{A_w} \boldsymbol{R}_i(\boldsymbol{U})\cdot\boldsymbol{n}\mathrm{d}\boldsymbol{S} = \boldsymbol{0} \end{aligned} \tag{6}$$

showing the contribution of the three surfaces of the conical control volume, with $\boldsymbol{U}_i$ the cell average of the state vector $\boldsymbol{U}$ and with the ALE conservative inviscid flux-vector of the BN equations in the normal direction $\boldsymbol{n}$:

$$\boldsymbol{F}^{\mathrm{ALE}}(\boldsymbol{U},\boldsymbol{v})\,\boldsymbol{n} = \begin{pmatrix} -\alpha_1\boldsymbol{v}\cdot\boldsymbol{n} \\ \alpha_k\rho_k(\boldsymbol{u}_k-\boldsymbol{v})\cdot\boldsymbol{n} \\ \alpha_k\rho_k\boldsymbol{u}_k(\boldsymbol{u}_k-\boldsymbol{v})\cdot\boldsymbol{n}+\alpha_k p_k\boldsymbol{n} \\ \alpha_k\rho_k e_k(\boldsymbol{u}_k-\boldsymbol{v})\cdot\boldsymbol{n}+\alpha_k p_k\boldsymbol{u}_k\cdot\boldsymbol{n} \end{pmatrix}$$

Here $\boldsymbol{R}_i(\boldsymbol{U})$ is a function designed such that its integral over the surface of $\partial C_i(t)$ approximates the effect of the volume integral over $C_i(t)$ of the non-conservative terms $\boldsymbol{H}(\boldsymbol{U})\nabla\alpha_1$; i.e. the non-conservative term is discretized [39] using the following approximation:

$$\int_{A_{i+1/2}} \boldsymbol{R}_i(\boldsymbol{U}) \cdot \boldsymbol{n}_{i+1/2} \mathrm{d}\boldsymbol{S} + \int_{A_{i-1/2}} \boldsymbol{R}_i(\boldsymbol{U}) \cdot \boldsymbol{n}_{i-1/2} \mathrm{d}\boldsymbol{S} + \int_{A_w} \boldsymbol{R}_i(\boldsymbol{U}) \cdot \boldsymbol{n} \mathrm{d}\boldsymbol{S} \approx \int_{C_i} \boldsymbol{H}(\boldsymbol{U}) \nabla\alpha_1 \mathrm{d}V$$

The surface A_w corresponds to the moving pipe sidewall where the following conditions $\boldsymbol{u}_k \cdot \boldsymbol{n} = \boldsymbol{v} \cdot \boldsymbol{n}$ for $k = 1, 2$ are respected. As a consequence, the ALE conservative flux-vector at the wall can be expressed as:

$$\boldsymbol{F}^{\mathrm{ALE}}(\boldsymbol{U}, \boldsymbol{v}) \cdot \boldsymbol{n}\Big|_{A_w} = \left.\begin{pmatrix} -\alpha_1 \boldsymbol{v} \cdot \boldsymbol{n} \\ 0 \\ \alpha_k p_k \boldsymbol{n} \\ \alpha_k p_k \boldsymbol{v} \cdot \boldsymbol{n} \end{pmatrix}\right|_{A_w}$$

For the two cross-sections orthogonal to the pipe axis, conservative numerical fluxes $\mathbb{F}_{i\pm1/2}$ are defined as the edge average of the ALE conservative flux-vector in the following manner:

$$\mathbb{F}_{i\pm1/2} \equiv \frac{1}{|A_{i\pm1/2}|} \int_{A_{i\pm1/2}} \boldsymbol{F}^{\mathrm{ALE}}(\boldsymbol{U}, \boldsymbol{v}_{i\pm1/2}) \boldsymbol{n}_{i\pm1/2} \mathrm{d}\boldsymbol{S}.$$

with the conservative fluxes defined for the three surfaces, consideration is given to the integration of the non-conservative terms of the BN model over the considered conical control volume. First, for the pipe sidewall, there is no jump of α_1 across a wall, especially when a mirror state is used for the numerical flux, so the non-conservative flux across the wall boundary A_w is set to be null:

$$\int_{A_w} \boldsymbol{R}_i(\boldsymbol{U}) \cdot \boldsymbol{n} \mathrm{d}\boldsymbol{S} = \boldsymbol{0}$$

and, for the two cross-sections, we define the non-conservative numerical fluxes $\mathbb{R}_{i,i\pm1/2}$ as the following edge average:

$$\mathbb{R}_{i,i\pm1/2} \equiv \frac{1}{|A_{i\pm1/2}|} \int_{A_{i\pm1/2}} \boldsymbol{R}_i(\boldsymbol{U}) \cdot \boldsymbol{n}_{i\pm1/2} \mathrm{d}\boldsymbol{S}.$$

Finally, the only contribution due to the pipe sidewall A_w lies in the corresponding ALE conservative flux-vector. As a consequence, new terms arise in the phasic volume fraction, momentum and energy equations. Thus defining the wall volume fractions $(\alpha_k)_w$ and the wall phasic pressures $(p_k)_w$ (to approximate the different components of the fluxes) as the following averages:

$$(\alpha_k)_w \int_{A_w} \boldsymbol{v} \cdot \boldsymbol{n} \mathrm{d}\boldsymbol{S} \equiv \int_{A_w} \alpha_k \boldsymbol{v} \cdot \boldsymbol{n} \mathrm{d}\boldsymbol{S} \quad \text{and} \quad (\alpha_k)_w (p_k)_w \int_{A_w} \boldsymbol{\mathcal{H}}(\boldsymbol{v}, \boldsymbol{n}) \mathrm{d}\boldsymbol{S} \equiv \int_{A_w} \alpha_k p_k \boldsymbol{\mathcal{H}}(\boldsymbol{v}, \boldsymbol{n}) \mathrm{d}\boldsymbol{S} \quad \text{with} \quad \boldsymbol{\mathcal{H}}(\boldsymbol{v}, \boldsymbol{n}) = \begin{pmatrix} 0 \\ 0 \\ \boldsymbol{n} \\ \boldsymbol{v} \cdot \boldsymbol{n} \end{pmatrix}$$

leads to the following Ordinary Differential Equation (ODE) for each cell C_i:

$$\frac{\mathrm{d}}{\mathrm{d}t}(|C_i|\boldsymbol{U}_i) + \mathbb{F}_{i+1/2}|A_{i+1/2}| + \mathbb{F}_{i-1/2}|A_{i-1/2}| + \mathbb{R}_{i,i+1/2}|A_{i+1/2}| + \mathbb{R}_{i,i-1/2}|A_{i-1/2}| + \boldsymbol{\Upsilon}_i = \boldsymbol{0} \tag{7}$$

with $\boldsymbol{\Upsilon}_i$ the term derived from the pipe sidewall in cell C_i given by:

$$\boldsymbol{\Upsilon}_i = \int_{A_w} \boldsymbol{F}^{\mathrm{ALE}}(\boldsymbol{U}, \boldsymbol{v}) \boldsymbol{n} \mathrm{d}\boldsymbol{S}.$$

This term must be expressed using numerical quantities associated with the two cross-sections orthogonal to the pipe/flow axis. For this purpose, the Surface Conservation Law (SCL) and the Geometrical Conservation Law (GCL)

for the conical closed volume $C_i(t)$ are considered to express the different components of $\boldsymbol{\Upsilon}_i$ in the following manner:

$$\left\{\begin{array}{lcll} \displaystyle\int_{A_w} \boldsymbol{n}\mathrm{d}\boldsymbol{S} & = & \displaystyle -\left(\int_{A_{i+1/2}} \boldsymbol{n}_{i+1/2}\mathrm{d}\boldsymbol{S} + \int_{A_{i-1/2}} \boldsymbol{n}_{i-1/2}\mathrm{d}\boldsymbol{S}\right) & = -\left(\boldsymbol{n}_{i+1/2}|A_{i+1/2}| + \boldsymbol{n}_{i-1/2}|A_{i-1/2}|\right) \\ \displaystyle\int_{A_w} \boldsymbol{v}\cdot\boldsymbol{n}\mathrm{d}\boldsymbol{S} & = & \displaystyle \frac{\mathrm{d}}{\mathrm{d}t}|C_i| - \left(\int_{A_{i+1/2}} \boldsymbol{v}_{i+1/2}\cdot\boldsymbol{n}_{i+1/2}\mathrm{d}\boldsymbol{S} + \int_{A_{i-1/2}} \boldsymbol{v}_{i-1/2}\cdot\boldsymbol{n}_{i-1/2}\mathrm{d}\boldsymbol{S}\right) & = \displaystyle\frac{\mathrm{d}}{\mathrm{d}t}|C_i| - \left(v_{i+1/2}|A_{i+1/2}| + v_{i-1/2}|A_{i-1/2}|\right) \end{array}\right.$$

with $v_{i+1/2} = \boldsymbol{v}_{i+1/2}\cdot\boldsymbol{n}_{i+1/2}$. Equation (7) is then integrated in time using the explicit Euler scheme leading to:

$$|C_i^{n+1}|\boldsymbol{U}_i^{n+1} - |C_i^n|\boldsymbol{U}_i^n + \Delta t^n\left(\boldsymbol{\mathcal{F}}_{i+1/2}|A_{i+1/2}^{n+1/2}| + \boldsymbol{\mathcal{F}}_{i-1/2}|A_{i-1/2}^{n+1/2}| + \boldsymbol{\mathcal{R}}_{i,i+1/2}|A_{i+1/2}^{n+1/2}| + \boldsymbol{\mathcal{R}}_{i,i-1/2}|A_{i-1/2}^{n+1/2}|\right) + \boldsymbol{\Upsilon}_i^n = \boldsymbol{0} \tag{8}$$

with $\boldsymbol{\mathcal{F}}_{i\pm1/2}$ the conservative numerical fluxes approximating the edge average $\mathbb{F}_{i\pm1/2}$ which can be written as:

$$\boldsymbol{\mathcal{F}}_{i\pm1/2} = \begin{pmatrix} \left(\mathcal{F}_1^{(0)}\right)_{i\pm1/2} \\ \left(\mathcal{F}_k^{(1)}\right)_{i\pm1/2} \\ \left(\boldsymbol{\mathcal{F}}_k^{(2)}\right)_{i\pm1/2} \\ \left(\mathcal{F}_k^{(3)}\right)_{i\pm1/2} \end{pmatrix} \tag{9}$$

where the components $\left(\mathcal{F}_k^{(0)}\right)_{i\pm1/2}$, $\left(\mathcal{F}_k^{(1)}\right)_{i\pm1/2}$, $\left(\boldsymbol{\mathcal{F}}_k^{(2)}\right)_{i\pm1/2}$ and $\left(\mathcal{F}_k^{(3)}\right)_{i\pm1/2}$ correspond to the volume fraction, mass, momentum and energy conservative numerical fluxes of phase k, respectively, and with $\boldsymbol{\mathcal{R}}_{i,i\pm1/2}$ the non-conservative numerical fluxes approximating the edge average $\mathbb{R}_{i,i\pm1/2}$ which can be written as:

$$\boldsymbol{\mathcal{R}}_{i,i\pm1/2} = \begin{pmatrix} \left(\mathcal{R}_1^{(0)}\right)_{i,i\pm1/2} \\ 0 \\ \left(\boldsymbol{\mathcal{R}}_k^{(2)}\right)_{i,i\pm1/2} \\ \left(\mathcal{R}_k^{(3)}\right)_{i,i\pm1/2} \end{pmatrix} \tag{10}$$

where the components $\left(\mathcal{R}_k^{(0)}\right)_{i,i\pm1/2}$, $\left(\boldsymbol{\mathcal{R}}_k^{(2)}\right)_{i,i\pm1/2}$ and $\left(\mathcal{R}_k^{(3)}\right)_{i,i\pm1/2}$ correspond to the volume fraction, momentum and energy non-conservative numerical fluxes of phase k, respectively. In addition, using both SCL and GCL, the term $\boldsymbol{\Upsilon}_i^n$ derived from the pipe sidewall can be expressed as:

$$\boldsymbol{\Upsilon}_i^n = \begin{pmatrix} -(\alpha_1)_w\,\mathcal{T}_i^n \\ 0 \\ -(\alpha_k)_w\,(p_k)_w\,\boldsymbol{\mathcal{S}}_i^n \\ (\alpha_k)_w\,(p_k)_w\,\mathcal{T}_i^n \end{pmatrix} \quad \text{with} \quad \left\{\begin{array}{lcl} \mathcal{T}_i^n & = & |C_i^{n+1}| - |C_i^n| - \Delta t^n\left(v_{i+1/2}^{n+1/2}|A_{i+1/2}^{n+1/2}| + v_{i-1/2}^{n+1/2}|A_{i-1/2}^{n+1/2}|\right) \\ \boldsymbol{\mathcal{S}}_i^n & = & \Delta t^n\left(\boldsymbol{n}_{i+1/2}^{n+1/2}|A_{i+1/2}^{n+1/2}| + \boldsymbol{n}_{i-1/2}^{n+1/2}|A_{i-1/2}^{n+1/2}|\right) \end{array}\right.$$

where $\boldsymbol{n}_{i\pm1/2}^{n+1/2}$, $|A_{i\pm1/2}^{n+1/2}|$ and $v_{i\pm1/2}^{n+1/2}$ are a weighted average of the n and $n+1$ time level areas of the unit outward normal vector, the interfaces and the grid velocity, respectively in order to implicitly verify both the Discrete Surface Conservation Law and the Discrete Geometrical Conservation Law as in [44, 45, 46, 39]. For clarity, the subscript $n+1/2$ used for the geometrical variables (surface, volume, unit outward normal vector, grid velocity...) is omitted in the following.

Realistic piping configurations are usually modelled as flow networks characterized by the presence of several pipes (or branches) connected to specific points (called junctions in the following) leading to potentially complex networks with several junctions and branches. For the numerical calculation of flow networks, it is convenient to consider an arbitrary orientation of each single pipe. So the local orientation of each control volume is here considered. For this purpose, a unit vector $\boldsymbol{m}_i$ associated with the local orientation of the conical cell C_i and collinear to the pipe axis is introduced. As in [1], when considering two adjacent cells denoted here by C_i and C_{i+1}, there are 4 different configurations, represented in Fig. (2), depending on the orientation of the cell C_i with respect to the one of the cell

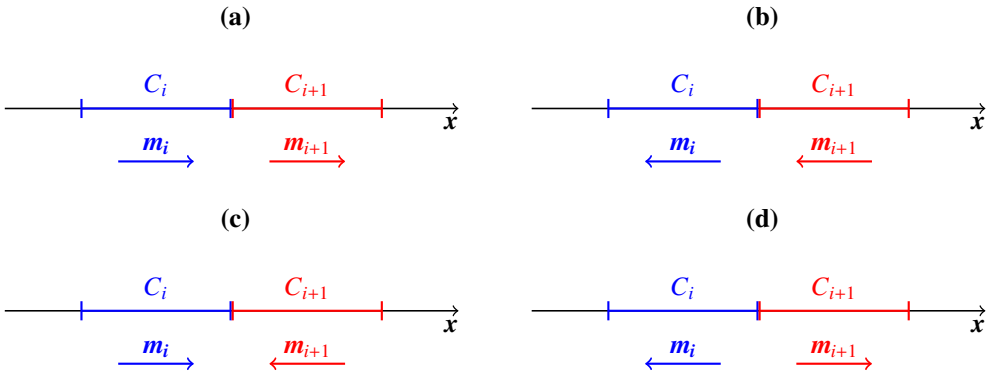

Figure 2: Sketch-up of the different configurations for the arbitrary orientation of two adjacent cells denoted C_i and C_{i+1}.

C_{i+1}. The discrete multi-dimensional momentum equation is then projected to the unit vector $\boldsymbol{m}_i$ leading to:

$$\begin{aligned} |C_i^{n+1}|\,(\alpha_k\rho_k u_k)_i^{n+1} - |C_i^n|\,(\alpha_k\rho_k u_k)_i^n \quad &+ \quad \Delta t^n\left[\left(\mathcal{F}_k^{(2)}\right)_{i+1/2}\cdot\boldsymbol{m}_i|A_{i+1/2}| + \left(\mathcal{F}_k^{(2)}\right)_{i-1/2}\cdot\boldsymbol{m}_i|A_{i-1/2}|\right] \\ &+ \quad \Delta t^n\left[\left(\mathcal{R}_k^{(2)}\right)_{i,i+1/2}\cdot\boldsymbol{m}_i|A_{i+1/2}| + \left(\mathcal{R}_k^{(2)}\right)_{i,i-1/2}\cdot\boldsymbol{m}_i|A_{i-1/2}|\right] \\ &- \quad (\alpha_k)_w\,(p_k)_w\,\Delta t^n\left(\delta^i_{i+1/2}|A_{i+1/2}| + \delta^i_{i-1/2}|A_{i-1/2}|\right) = 0 \end{aligned}$$

with $(u_k)_i = (\boldsymbol{u}_k)_i\cdot\boldsymbol{m}_i$ and $\delta^i_{i\pm1/2} = \boldsymbol{n}_{i\pm1/2}\cdot\boldsymbol{m}_i$. Note that $\delta^i_{i+1/2} = \pm1$, the sign of $\delta^i_{i+1/2}$ depends on the orientation of the conical cell C_i with respect to the outward unit vector $\boldsymbol{n}_{i+1/2}$. As only quasi 1-D flows are considered here, the phasic velocity vector $(\boldsymbol{u}_k)_i$ is collinear to the pipe axis $\boldsymbol{m}_i$ leading to: $(\boldsymbol{u}_k)_i = (u_k)_i\,\boldsymbol{m}_i$ and thus $(u_k)_i = (\boldsymbol{u}_k)_i\cdot\boldsymbol{m}_i$, the other velocity components being neglected.

2.1.3. 1-D discrete Baer-Nunziato equations of one single pipe

Finally, the system of discrete Baer-Nunziato equations for a single pipe with varying cross-section is:

$$|C_i^{n+1}|\boldsymbol{Q}_i^{n+1} - |C_i^n|\boldsymbol{Q}_i^n + \Delta t^n\left(\boldsymbol{\Phi}^i_{i+1/2}|A_{i+1/2}| + \boldsymbol{\Phi}^i_{i-1/2}|A_{i-1/2}| + \boldsymbol{\Pi}_{i,i+1/2}|A_{i+1/2}| + \boldsymbol{\Pi}_{i,i-1/2}|A_{i-1/2}|\right) + \boldsymbol{\Psi}_i^n = \boldsymbol{0} \qquad (11)$$

with

$$\boldsymbol{Q}_i = \begin{pmatrix} \alpha_1 \\ \alpha_k\rho_k \\ \alpha_k\rho_k u_k \\ \alpha_k\rho_k e_k \end{pmatrix}_i, \quad \boldsymbol{\Phi}^i_{i\pm1/2} = \begin{pmatrix} -(\alpha_1)_{i\pm1/2}\,v_{i\pm1/2} \\ \left(\mathcal{F}_k^{(1)}\right)_{i\pm1/2} \\ \left(\mathcal{F}_k^{(2)}\right)_{i\pm1/2}\cdot\boldsymbol{m}_i \\ \left(\mathcal{F}_k^{(3)}\right)_{i\pm1/2} \end{pmatrix}, \quad \boldsymbol{\Pi}_{i,i\pm1/2} = \begin{pmatrix} \left(\mathcal{R}_1^{(0)}\right)_{i,i\pm1/2} \\ 0 \\ \left(\mathcal{R}_k^{(2)}\right)_{i,i\pm1/2}\cdot\boldsymbol{m}_i \\ \left(\mathcal{R}_k^{(3)}\right)_{i,i\pm1/2} \end{pmatrix}$$

$$\text{and} \quad \boldsymbol{\Psi}_i^n = \begin{pmatrix} -(\alpha_1)_w\,\mathcal{T}_i^n \\ 0 \\ -(\alpha_k)_w\,(p_k)_w\,\mathcal{S}_i^n \\ (\alpha_k)_w\,(p_k)_w\,\mathcal{T}_i^n \end{pmatrix} \quad \text{where} \quad \mathcal{S}_i^n = \boldsymbol{\mathcal{S}}_i^n\cdot\boldsymbol{m}_i$$

The variation of cross-section is involved in the non-conservative term $\boldsymbol{\Psi}_i^n$. Note that this corresponds to a discrete form of the following continuous counterpart:

$$\left\{\begin{array}{lllllll} \partial_t(\alpha_1 A) & & & + & u_I A\partial_x\alpha_1 & = & \alpha_1\partial_t A \\ \partial_t(\alpha_k\rho_k A) & + & \partial_x(\alpha_k\rho_k u_k A) & & & = & 0 \\ \partial_t(\alpha_k\rho_k u_k A) & + & \partial_x\left(\alpha_k\rho_k u_k^2 A + \alpha_k p_k A\right) & - & p_I A\partial_x\alpha_k & = & \alpha_k p_k\partial_x A \\ \partial_t(\alpha_k\rho_k e_k A) & + & \partial_x(\alpha_k\rho_k e_k u_k A + \alpha_k p_k u_k A) & - & p_I u_I A\partial_x\alpha_k & = & -\alpha_k p_k\partial_t A \end{array}\right. \qquad (12)$$

We can observe that, aside from symmetrizing closures, this set of equations corresponds to the one used in the RELAP-7 theory manual [28], except that here the time variation of the cross-section is considered for taking into

account the pipe hoop elasticity for example. First, note that in the case that the cross-section is constant, Eq. (11) gives the classical 1-D Baer-Nunziato system. Then, in the case where α_1 is constant, Eq. (11) reduces to two sets of Euler equations in variable cross-section.
The numerical fluxes $\mathbf{\Phi}^i_{i\pm1/2}$ are the 1-D projection of the 3-D conservative numerical flux $\boldsymbol{\mathcal{F}}_{i\pm1/2}$ on the cell C_i following its local orientation $\boldsymbol{m}_i$:

$$\mathbf{\Phi}^i_{i\pm1/2} = \mathcal{P}_i\left(\boldsymbol{\mathcal{F}}_{i\pm1/2}, \boldsymbol{m}_i\right) \quad \text{with} \quad \mathcal{P}_i\left(\begin{pmatrix} \left(G_1^{(0)}\right) \\ \left(G_k^{(1)}\right) \\ \left(\boldsymbol{G}_k^{(2)}\right) \\ \left(G_k^{(3)}\right) \end{pmatrix}, \boldsymbol{m}_i\right) = \begin{pmatrix} \left(G_1^{(0)}\right) \\ \left(G_k^{(1)}\right) \\ \left(\boldsymbol{G}_k^{(2)}\right)\cdot \boldsymbol{m}_i \\ \left(G_k^{(3)}\right) \end{pmatrix} \tag{13}$$

with $\mathcal{P}_i$ the 1-D projection operator using the same notations as those introduced in [1]. In the same manner, the non-conservative numerical fluxes $\mathbf{\Pi}_{i,i\pm1/2}$ are the 1-D projection of the 3-D non-conservative numerical flux $\boldsymbol{\mathcal{R}}_{i,i\pm1/2}$ of the BN equations on the cell C_i:

$$\mathbf{\Pi}_{i,i\pm1/2} = \mathcal{P}_i\left(\boldsymbol{\mathcal{R}}_{i,i\pm1/2}, \boldsymbol{m}_i\right) \tag{14}$$

In the same way, $\boldsymbol{Q}_i$ is the 1-D projection of the state vector $\boldsymbol{U}_i$ on cell C_i:

$$\boldsymbol{Q}_i = \mathcal{P}_i\left(\boldsymbol{U}_i, \boldsymbol{m}_i\right) \tag{15}$$

In addition, the inverse operator $\mathcal{E}_i$ can also be defined:

$$\mathcal{E}_i\left(\begin{pmatrix} \left(H_1^{(0)}\right) \\ \left(H_k^{(1)}\right) \\ \left(H_k^{(2)}\right) \\ \left(H_k^{(3)}\right) \end{pmatrix}, \boldsymbol{m}_i\right) = \begin{pmatrix} \left(H_1^{(0)}\right) \\ \left(H_k^{(1)}\right) \\ \left(H_k^{(2)}\right)\boldsymbol{m}_i \\ \left(H_k^{(3)}\right) \end{pmatrix} \tag{16}$$

Notice that the following identity is always satisfied:

$$\boldsymbol{Q}_i = \mathcal{P}_i\left[\mathcal{E}_i\left(\boldsymbol{Q}_i, \boldsymbol{m}_i\right), \boldsymbol{m}_i\right] \tag{17}$$

In addition, as the considered geometry is quasi-1D, i.e. the phasic velocity vector $(\boldsymbol{u}_k)_i$ is collinear to the pipe axis $\boldsymbol{m}_i$: $(\boldsymbol{u}_k)_i = (u_k)_i\,\boldsymbol{m}_i$, the following relation is also satisfied:

$$\boldsymbol{U}_i = \mathcal{E}_i\left[\mathcal{P}_i\left(\boldsymbol{U}_i, \boldsymbol{m}_i\right), \boldsymbol{m}_i\right] \tag{18}$$

The surfaces $|A_{i\pm1/2}|$ are expressed using the inner diameters of the corresponding pipe cell, i.e. $|A_{i\pm1/2}| = \pi d^2_{i\pm1/2}/4$. The conical volume $|C_i|$ is computed as follows:

$$|C_i| = \frac{\pi h_i}{12}\left(d^2_{i+1/2} + d_{i+1/2}d_{i-1/2} + d^2_{i-1/2}\right)$$

with h_i the length of the control volume C_i.

The time step Δt^n used in the explicit scheme in Eq. (11) is given using the Courant number:

$$C \equiv \Delta t^n \max_i\left(\frac{(r_{\boldsymbol{A}})^n_i}{l^n_i}\right) \tag{19}$$

where $r_{\boldsymbol{A}}$ is the spectral radius of the convective Jacobian including both conservative and non-conservative terms (in 1-D, $r_{\boldsymbol{A}} = \max_k\left(|u_k| + c_k\right)$) with c_k the phasic speed of sound given by the EOS and l^n_i the characteristic length of the conical cell C^n_i. For single pipes, l^n_i is set to be equal to h^n_i the length of C^n_i.
The conservative and non-conservative numerical fluxes denoted by $\mathbf{\Phi}^i_{i\pm1/2}$ and $\mathbf{\Pi}_{i,i\pm1/2}$ respectively, as well as the wall fluxes denoted by $(\alpha_k)_w$ and $(p_k)_w$ in Eq. (11) have now been expressed. The remaining numerical challenge is to ensure the well-balanced property of the global numerical scheme with respect to both volume fraction and cross-section variations.

2.1.4. Numerical discretization

The conservative numerical flux $\mathbf{\Phi}^{i}_{i+1/2}$ and the non-conservative numerical term $\mathbf{\Pi}_{i,i+1/2}$ are here expressed using the HLLC-type scheme proposed by Tokareva and Toro [37] for the BN equations. This approximate Riemann solver takes into account all of the six characteristic fields present in the exact solution of the Riemann problem. For the phasic genuinely non-linear waves, as there is no change of volume fractions, averaged Rankine-Hugoniot conditions are used as in the classical case of the HLLC scheme for the Euler equations. For the phasic linearly degenerate waves, the Riemann invariants are preserved for the computation of intermediate states. In addition, the thin-layer approximation proposed by Schwendeman *et al.* [36] is used for the contact discontinuity u_I to compute the non-conservative terms. Finally, this results in a non-linear algebraic system which is solved using a Newton-Raphson method. Further details on the numerical discretization used here are given in [39] where both "subsonic" and "supersonic" wave configurations are considered. To bypass the iterative resolution required in the HLLC scheme, some approximations can be used as detailed in [40] for the subsonic configuration but are not considered in the following.
In addition, the wall phasic pressures and volume fractions are taken to be equal to their cell-averaged counterpart: i.e. $(p_k)_w = (p_k)^n_i$ and $(\alpha_k)_w = (\alpha_k)^n_i$.
The first-order accuracy in time and in space is obtained using $\boldsymbol{Q}_L = \boldsymbol{Q}^n_i$ and $\boldsymbol{Q}_R = \boldsymbol{Q}^n_{i+1}$.

2.1.5. Pipe connections modeling

For the numerical modeling of flow networks, the boundary conditions of several pipe flows have to be specified at the junctions in a correct manner as improper specifications contaminate all the flow. For this purpose, the numerical procedure detailed in [22, 23, 1] in the context of the Euler equations is here extended to the Baer-Nunziato two-phase flow models with the inherent difficulties due to the presence of non-conservative terms. The junction of several pipes is here modeled using a unique three-dimensional fictitious cell connecting the different branched pipes. As a consequence, the 3-D Baer-Nunziato equations are solved in the junction cell and thus, as done previously for the Euler equations, the junction problem consists in coupling the connected 1-D pipes and the 3-D junction through the numerical fluxes at the common edges between the branched pipes and the junction. In the same spirit, Bellamoli *et al.* [47, 48] have proposed to represent the junction of several pipes by the real geometry of the junction using the multi-dimension equations on one or more unstructured cells at the junction and its vicinity in the context of shallow-water channels.

The notations introduced in [1] for the geometrical quantities associated with the junction of several pipes are employed here. As represented in Fig. (3), the junction is modeled using a 3-D cell C_j surrounded by common interfaces with adjacent branch cells and wall surfaces. Let us consider the general case of a junction connecting N pipes of arbitrary cross-sectional areas and arbitrary flow/pipe directions. The common interfaces with the branched pipes are denoted here A_l for $l = 1, ...N$ and the wall surfaces are replaced by an equivalent wall surface denoted A_w. As a consequence, the boundary ∂C_j of the junction cell can be decomposed as:

$$\partial C_j = \left(\bigcup_{l \in \mathcal{V}} A_l \right) \bigcup A_w$$

with $\mathcal{V}$ the set of the surfaces of the junction cell linked to a 1-D pipeline. In the particular case of the connection of two pipes with the same inner diameter, there is no wall surface at the junction. The 1-D adjacent pipe cell branched to the junction through the edge A_l is denoted here by C_{il}. By construction, the unit outward vectors of C_{il} and C_j by the common edge A_l are opposite, i.e. $\boldsymbol{n}_{j,l} = -\boldsymbol{n}_{il,l}$. The derivation of the representative wall-fluxes are now expressed as a function of the ones of the 1-D pipes adjacent to the junction. For this purpose, the SCL relation for the edges of the closed 3-D junction cell C_j is used as in the previous section leading to:

$$\int_{\partial C_j} \boldsymbol{n} \mathrm{d}\boldsymbol{S} = \boldsymbol{0} \qquad \Rightarrow \qquad \int_{A_w} \boldsymbol{n} \mathrm{d}\boldsymbol{S} = \sum_{l \in \mathcal{V}} \boldsymbol{n}_{il,l} |A_l|$$

As in the ALE formulation of the junction finite-volume treatment proposed previously [1] for the Euler equations, all of the junction surfaces are assumed to have the same displacement (i.e. which corresponds to a rigid body motion).

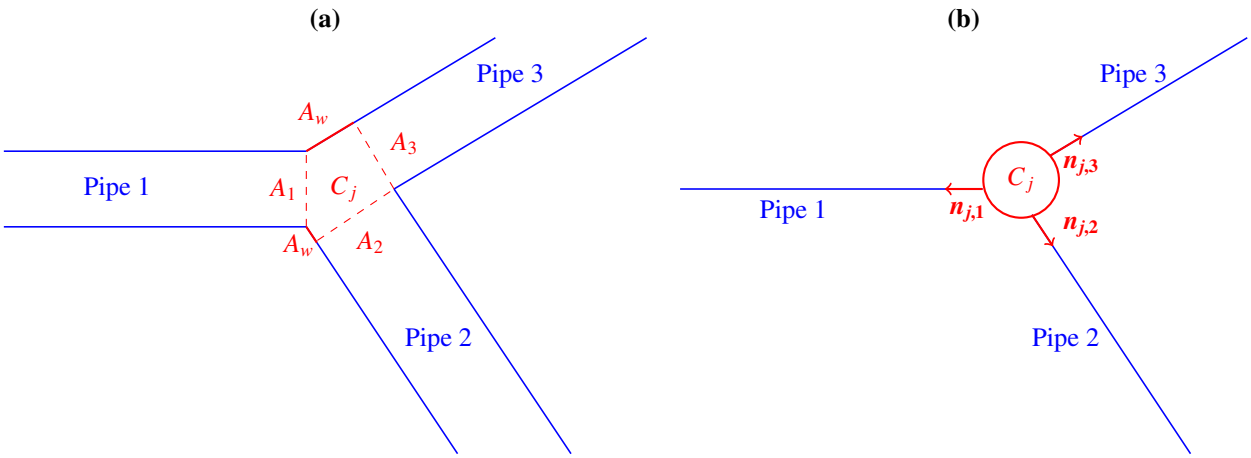

Figure 3: Sketch of the junction of N pipes: **(a)** real 3-D case; **(b)** ghost junction cell C_j connecting the different pipes.

Application of the GCL to the 3-D junction cell C_j gives:

$$\int_{\partial C_j} \boldsymbol{v}\cdot\boldsymbol{n}\mathrm{d}\boldsymbol{S}=0 \quad \Rightarrow \quad \int_{A_w} \boldsymbol{v}\cdot\boldsymbol{n}\mathrm{d}\boldsymbol{S}=\sum_{l\in\mathcal{V}} v_{il,l}|A_l| \quad \text{and} \quad |C_j^{n+1}|=|C_j^n|\Big(\equiv|C_j|\Big) \quad \text{i.e.} \quad \frac{\mathrm{d}}{\mathrm{d}t}|C_j|=0$$

with $v_{il,l}=\boldsymbol{v}_l\cdot\boldsymbol{n}_{il,l}$.
Then, the multi-dimensional Baer-Nunziato equations given in Eq. (1) are considered for the junction and are integrated over the junction cell C_j. The conservative and non-conservative numerical fluxes at the junction interfaces and the wall-flux are thus used to update the flow variables of the multi-dimensional junction cell. Once again, the use of SCL and GCL makes it possible to express the equivalent wall-flux as a function of geometrical quantities at common interfaces between the junction and the branched pipes as:

$$|C_j|\boldsymbol{U}_j^{n+1}-|C_j|\boldsymbol{U}_j^n+\Delta t^n\sum_{l\in\mathcal{V}}\boldsymbol{\mathcal{F}}_{j,l}|A_l|+\Delta t^n\sum_{l\in\mathcal{V}}\boldsymbol{\mathcal{R}}_{j,l}|A_l|+\Delta t^n\sum_{l\in\mathcal{V}}\boldsymbol{G}_{il,l}|A_l|=\boldsymbol{0} \quad \text{with} \quad \boldsymbol{G}_{il,l}=\begin{pmatrix}-(\alpha_1)_w\,v_{il,l}\\ 0\\ (\alpha_k)_w\,(p_k)_w\,\boldsymbol{n}_{il,l}\\ (\alpha_k)_w\,(p_k)_w\,v_{il,l}\end{pmatrix}$$

$\boldsymbol{\mathcal{F}}_{j,l}$ is the 3-D outward conservative numerical fluxes with respect to C_j at the edge A_l for $l\in\mathcal{V}$. This interface conservative flux at the edge A_l is expressed as the 3-D extension of the boundary flux of the neighboring branch C_{il} using the conservative property of the fluxes as:

$$\boldsymbol{\mathcal{F}}_{j,l}=-\boldsymbol{\mathcal{F}}_{il,l} \tag{20}$$

In addition, the wall phasic pressure $(p_k)_w$ and the wall volume fraction $(\alpha_k)_w$ are set equal to the phasic cell-averaged pressure $(p_k)_j$ and the cell-averaged volume fraction $(\alpha_k)_j$ of the junction cell, respectively. This leads to:

$$|C_j|\boldsymbol{U}_j^{n+1}-|C_j|\boldsymbol{U}_j^n-\Delta t^n\sum_{l\in\mathcal{V}}\boldsymbol{\mathcal{F}}_{il,l}|A_l|+\Delta t^n\sum_{l\in\mathcal{V}}\boldsymbol{\mathcal{R}}_{j,l}|A_l|+\Delta t^n\sum_{l\in\mathcal{V}}\boldsymbol{G}_{il,l}|A_l|=\boldsymbol{0} \tag{21}$$

The conservative numerical flux $\boldsymbol{\mathcal{F}}_{il,l}$ at the interface between the multi-dimensional junction cell and the one-dimensional neighboring branch cell is expressed using the left and right states of the interface A_l, $\boldsymbol{U}_L$ and $\boldsymbol{U}_R$ respectively, the interface velocity $\boldsymbol{v}_l$ and the outward unit vector $\boldsymbol{n}_{il,l}$:

$$\boldsymbol{\mathcal{F}}_{il,l}=\boldsymbol{\mathcal{F}}\left(\boldsymbol{U}_L,\boldsymbol{U}_R,\boldsymbol{v}_l,\boldsymbol{n}_{il,l}\right)$$

The first-order accuracy in time and space is obtained with:

$$\boldsymbol{U}_L = \mathcal{E}_{il}\left(\boldsymbol{Q}_{il}^n, \boldsymbol{m}_{il}\right) \text{ and } \boldsymbol{U}_R = \boldsymbol{U}_j^n \tag{22}$$

the left state corresponding to the 3-D extension of the 1-D state vector of the pipe cell C_{il} (see Eq. (16)) and the right state to the cell average of the conservative variables at the junction. In the same manner, the non-conservative numerical flux $\boldsymbol{\mathcal{R}}_{j,l}$ at the junction cell are expressed as:

$$\boldsymbol{\mathcal{R}}_{j,l} = \boldsymbol{\mathcal{R}}_j\left(\boldsymbol{U}_L, \boldsymbol{U}_R, \boldsymbol{v}_l, \boldsymbol{n}_{il,l}\right) \quad \text{with} \quad \boldsymbol{U}_L = \mathcal{E}_{il}\left(\boldsymbol{Q}_{il}^n, \boldsymbol{m}_{il}\right) \text{ and } \boldsymbol{U}_R = \boldsymbol{U}_j^n$$

Hong and Kim [22] have shown in the Euler equations framework that the classical choice given in Eq. (22) leads to the generation of spurious pressure jumps at the junction. In particular, they have demonstrated that this change in pressure across the interface of the junction is due to the variation of the normal velocity at this interface. Hong and Kim developed a non-dimensional scaling function to alleviate the interface flux [22]. In practice, only the normal velocity is conservatively reconstructed to scale the difference of the normal velocity component at the right state $\boldsymbol{U}_R$ associated with the junction cell. For the BN equations, this is done changing the phasic velocities as:

$$\begin{cases} (\alpha_k)_R &= (\alpha_k)_j^n \\ (\rho_k)_R &= (\rho_k)_j^n \\ (\boldsymbol{u}_k)_R &= (\tilde{u}_k)_R\, \boldsymbol{n}_{il,l} + \displaystyle\sum_d \left((\boldsymbol{u}_k)_j^n \cdot \boldsymbol{t}_{il,l}^{(d)}\right) \boldsymbol{t}_{il,l}^{(d)} \\ (p_k)_R &= (p_k)_j^n \end{cases} \quad \text{with } (\tilde{u}_k)_R = (\boldsymbol{u}_k)_{il}^n \cdot \boldsymbol{n}_{il,l} - (\mathcal{G}_k)_{il,l}\left((\boldsymbol{u}_k)_{il}^n \cdot \boldsymbol{n}_{il,l} - (\boldsymbol{u}_k)_j^n \cdot \boldsymbol{n}_{il,l}\right) \tag{23}$$

where $(\boldsymbol{u}_k)_{il}^n \cdot \boldsymbol{n}_{il,l} = (u_k)_{il}^n\, \delta_{il,l}^{il}$ with $\delta_{il,l}^{il} = \boldsymbol{m}_{il} \cdot \boldsymbol{n}_{il,l}$ and $\boldsymbol{t}_{il,l}^{(d)}$ for $d = 1, 2$ are the unit tangent vectors of the considered surface. The phasic scaling function $(\mathcal{G}_k)_{il,l}$ for each phasic velocity corresponding to the one proposed by Hong and Kim [22] in the context of the Euler equations is given by:

$$(\mathcal{G}_k)_{il,l} = \frac{1}{2}\left[1 - \text{sign}\left((u_k)_{il}^n\, \delta_{il,l}^{il}\right)\right] \min\left(\frac{|\,(\boldsymbol{u}_k)_{il}^n \cdot \boldsymbol{n}_{il,l} - (\boldsymbol{u}_k)_j^n \cdot \boldsymbol{n}_{il,l}|}{(c_k)_{il,j}}, 1\right)$$

with $(c_k)_{il,j} = \max\left((c_k)_{il}^n, (c_k)_j^n\right)$. We can notice that $0 \leq (\mathcal{G}_k)_{il,l} \leq 1$. When $(\mathcal{G}_k)_{il,l} = 1$, the classical choice given in Eq. (22) is retrieved. However, when $(\mathcal{G}_k)_{il,l} = 0$, there is no jump of normal phasic velocity between the left and the right states of the corresponding junction interface.

Knowing the left and right states of the junction interface A_l obtained via $\boldsymbol{U}_L = \mathcal{E}_{il}\left(\boldsymbol{Q}_{il}^n, \boldsymbol{m}_{il}\right)$ and $\boldsymbol{U}_R$ given by Eq. (23), respectively, the conservative numerical flux $\boldsymbol{\mathcal{F}}_{il,l}$, the non-conservative flux $\boldsymbol{\mathcal{R}}_{j,l}$ as well as the wall-flux $\boldsymbol{G}_{il,l}$ can be computed making it possible to update the state variables vector $\boldsymbol{U}_j$ at the junction cell using Eq. (21). Afterwards, for the neighbor pipe C_{il}, the conservative flux $\boldsymbol{\mathcal{F}}_{il,l}$ is projected following the orientation of cell C_{il}. In addition, the 3-D non-conservative flux $\boldsymbol{\mathcal{R}}_{il,l}$ is also computed using the left and right states at the junction area and then projected following the orientation of cell C_{il}. The state vector $\boldsymbol{Q}_{il}$ is thus updated following Eq. (11) using the 1-D projected conservative and non-conservative numerical fluxes (see Eq. (13)):

$$\boldsymbol{\Phi}_{il,l}^{il} = \mathcal{P}_{il}\left(\boldsymbol{\mathcal{F}}_{il,l}, \boldsymbol{m}_{il}\right) \quad \text{and} \quad \boldsymbol{\Pi}_{il,l} = \mathcal{P}_{il}\left(\boldsymbol{\mathcal{R}}_{il,l}, \boldsymbol{m}_{il}\right)$$

As the present junction treatment is based on the integral form of the 3-D BN equations (see Eq. (21)), it is noted that in the case of the use of numerical fluxes which are EOS-independent, the method is able to tackle general EOS. In addition, the other advantage of the present method is that no iterative procedure is required. In addition, this approach is also used here to tackle the abrupt change of the cross-section in pipe systems where only two pipes with different cross-section meet at the junction.

Finally, the junction surfaces $|A_l|$ are expressed using the inner diameters of the corresponding adjacent 1-D pipe cells, i.e. $|A_l| = \pi d_l^2/4$. The size of the volume junction $|C_j|$ can be estimated as proposed in [1], using the inner diameters of the junction interfaces as:

$$|C_j| = \frac{4}{3}\pi r_j^3 \quad \text{with} \quad 4\pi r_j^2 \equiv \sum_{l \in \mathcal{V}} |A_l| \tag{24}$$

Other choices have been proposed in the literature, e.g. in Hong and Kim [22] where the average volume of neighboring cells is used as the volume of the junction cell. Finally, the corresponding characteristic length l_j of the junction cell C_j used in the time-step computation in Eq. (19) is set to be $l_j = r_j$.

2.1.6. Boundary conditions

The treatment of the boundary conditions in the present finite-volume scheme is based on the use of a ghost cell virtually created outside the computational domain where a fictitious state is used to compute the fluxes at the

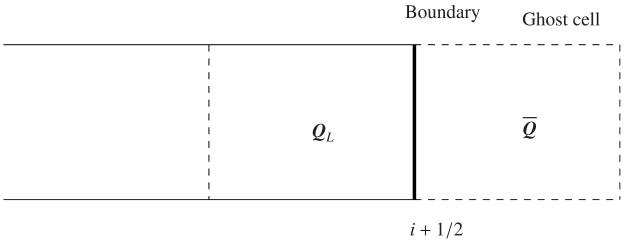

Figure 4: Sketch of a boundary condition at the interface denoted by $i+1/2$ with $\boldsymbol{Q}_L$ the state of the adjacent cell of the considered boundary and $\overline{\boldsymbol{Q}}$ the fictitious state of the corresponding ghost cell.

boundary. This fictitious state denoted here $\overline{\boldsymbol{Q}}$ is expressed in practice using the state denoted $\boldsymbol{Q}_L$ of the adjacent cell of the interface denoted here $i+1/2$ corresponding to the boundary as shown in Fig. (4). In the following, the orientation of the ghost cell is assumed to be the same as its adjacent cell. Finally, the conservative and non-conservative numerical fluxes are computed using the two states $\boldsymbol{Q}_L$ and $\overline{\boldsymbol{Q}}$. We describe how the fictitious state is computed for each boundary conditions.

The moving wall boundary condition is imposed using the mirror state:

$$\overline{(\alpha_k)} = (\alpha_k)_L\,, \quad \overline{(\rho_k)} = (\rho_k)_L\,, \quad \overline{(u_k)} = 2v_{i+1/2}\delta^L_{i+1/2} - (u_k)_L \quad \text{and} \quad \overline{(p_k)} = (p_k)_L \tag{25}$$

with $\delta^L_{i+1/2} = \boldsymbol{n}_{i+1/2} \cdot \boldsymbol{m}_L$.

The transmissive boundary condition is imposed via:

$$\overline{(\alpha_k)} = (\alpha_k)_L\,, \quad \overline{(\rho_k)} = (\rho_k)_L\,, \quad \overline{(u_k)} = (u_k)_L \quad \text{and} \quad \overline{(p_k)} = (p_k)_L \tag{26}$$

Time history of pressure can also be imposed via:

$$\overline{(\alpha_k)} = (\alpha_k)_L\,, \quad \overline{(\rho_k)} = (\rho_k)_L\,, \quad \overline{(u_k)} = (u_k)_L \quad \text{and} \quad \overline{(p_k)} = \mathcal{P}(t^n) \tag{27}$$

where $\mathcal{P}(t)$ is the imposed pressure at time t.

The "tank" condition is imposed following the two steps described below. First, the fictitious cell corresponding to the considered tank is associated to the initial prescribed phasic volume fractions $(\alpha_k)_{\text{tank}}$, densities $(\rho_k)_{\text{tank}}$, pressures $(p_k)_{\text{tank}}$ and volume $|C_{\text{tank}}|$. Then, for each 1-D pipe cell connected to the tank, the corresponding numerical flux directed outwardly from the pipe to the tank is computed using the following fictitious state:

$$\overline{(\alpha_k)} = (\alpha_k)_{\text{tank}}\,, \quad \overline{(\rho_k)} = (\rho_k)_{\text{tank}}\,, \quad \overline{(u_k)} = (u_k)_L \quad \text{and} \quad \overline{(p_k)} = (p_k)_{\text{tank}} \tag{28}$$

Finally, using this numerical flux, both the flow variables in the 1-D pipe cell and in the fictitious tank cell are updated. As the time evolution of the flow variables inside the tank is directly given by the ratio between this numerical flux and the volume $|C_{\text{tank}}|$, the size of this volume has a direct influence on the behavior of the tank. As a consequence, to ensure a constant pressure condition, i.e. corresponding to the prescribed initial values at the tank, a large size of the volume $|C_{\text{tank}}|$ should be prescribed as done in the following.

2.1.7. *Material model for the pipe wall elasticity*

The pressure wave problems considered here involve flows confined within a pipe. It is well know that the velocity of propagation of a wave in a pipe is distinctly different from the speed of sound in an unbounded fluid. As the fluid pressure increases, the fluid is not only compressed (with a concomitant density increase), but the pipe walls also expand elastically. Thus the density increase is less than it would be in the case of a confined flow in a rigid pipe. As a consequence, the elasticity of the pipe reduces the velocity of propagation of the pressure waves through it [49, 50, 16, 51]. This is referred to as the Korteweg [52] or Allievi [53] effect in the literature. For this purpose, Hooke's law is used to account for the pipe wall hoop elasticity. The expansion of the pipe circular cross-section is directly linked to the change of pressure following the linear equation [54]:

$$\frac{\mathrm{d}|A|}{|A|} = 2\beta\frac{\mathrm{d}p}{E} \quad \text{with} \quad \beta = \frac{1}{\left[(d+2\delta)^2 - d^2\right]}\left[(1-\nu_\mathrm{P})\,d^2 + (1+\nu_\mathrm{P})\,(d+2\delta)^2\right] \tag{29}$$

with d the inner diameter of the pipe, i.e. $|A| = \pi d^2/4$, δ the wall thickness which is assumed to be constant, E the Young's modulus of elasticity, ν_P the Poisson's ratio for the pipe material and p the mean pressure of the two-phase flow mixture given by: $p = \alpha_1 p_1 + \alpha_2 p_2$. The numerical integration of Eq. (29) is performed using the explicit Euler scheme as previously detailed in [1].

All of the algorithms described previously have been implemented in the fast transient dynamics software for fluids and structures *Europlexus* [55] (`http://www-epx.cea.fr/`) co-owned by the French *Commissariat à l'énergie atomique et aux énergies alternatives* (CEA) and by the European Commission. *Électricité de France* (EDF) is involved as a major partner of the consortium built for *Europlexus* software development.

3. Numerical tests

In order to demonstrate the potentiality of the proposed numerical method, several shock-tube and transient flow problems involving pipes junction, sudden change of duct cross-sections and elastic deformation of the pipe wall are considered. In addition, two experiments are also considered, the first one corresponds to a water-hammer with vapor cavity formation and collapse and the second one is a shock-tube in a network connected by a junction. All the computations are performed using the HLLC solver described in [39].

3.1. *Test 1: "Well-balanced" tests with an abrupt change of area*

Two "well-balanced" tests are proposed and the corresponding initial conditions are given in Table (1) using two perfect gases with $\gamma_1 = \gamma_2 = 1.4$. The first one similar to the one proposed in [1] in the single-phase context is

	Position	α_1	p_1 (Pa)	ρ_1 (kg.m^{-3})	u_1 (m.s^{-1})	p_2 (Pa)	ρ_2 (kg.m^{-3})	u_2 (m.s^{-1})	d (m)
(a)	$x \in [0;0.5]$	$1-10^{-6}$	10^5	1.2	0	10^5	1.2	0	10×10^{-3}
	$x \in [0.5;1]$	10^{-6}	10^5	1.2	0	10^5	1.2	0	15×10^{-3}
	Position	α_1	p_1 (Pa)	ρ_1 (kg.m^{-3})	u_1 (m.s^{-1})	p_2 (Pa)	ρ_2 (kg.m^{-3})	u_2 (m.s^{-1})	d (m)
(b)	$x \in [0;0.5]$	$1-10^{-6}$	10^5	1.2	4.5	10^5	1.2	4.5	10×10^{-3}
	$x \in [0.5;1]$	10^{-6}	10^5	1.2	2	10^5	1.2	2	15×10^{-3}

Table 1: Initial conditions for the two well-balanced Riemann problems: **(a)** steady case with a initial zero velocity and **(b)** non-steady case.

based on a zero initial velocity in contrast to the second one. A 1-m long pipe is considered as rigid and transmissive boundary conditions are used at the inlet and outlet of the tube. A discontinuity of the duct cross-section is located at $x = 0.5$ m. This abrupt change of area is tackled using the finite-volume treatment of the pipe connections described previously. The computations are done with 200 cells and with the Courant number $C = 0.99$. The numerical solutions are displayed on Fig. (5) showing the well-balanced property of the present numerical approach even with a significant jump of the volume fraction α_1 in conjunction with a sudden change of area.

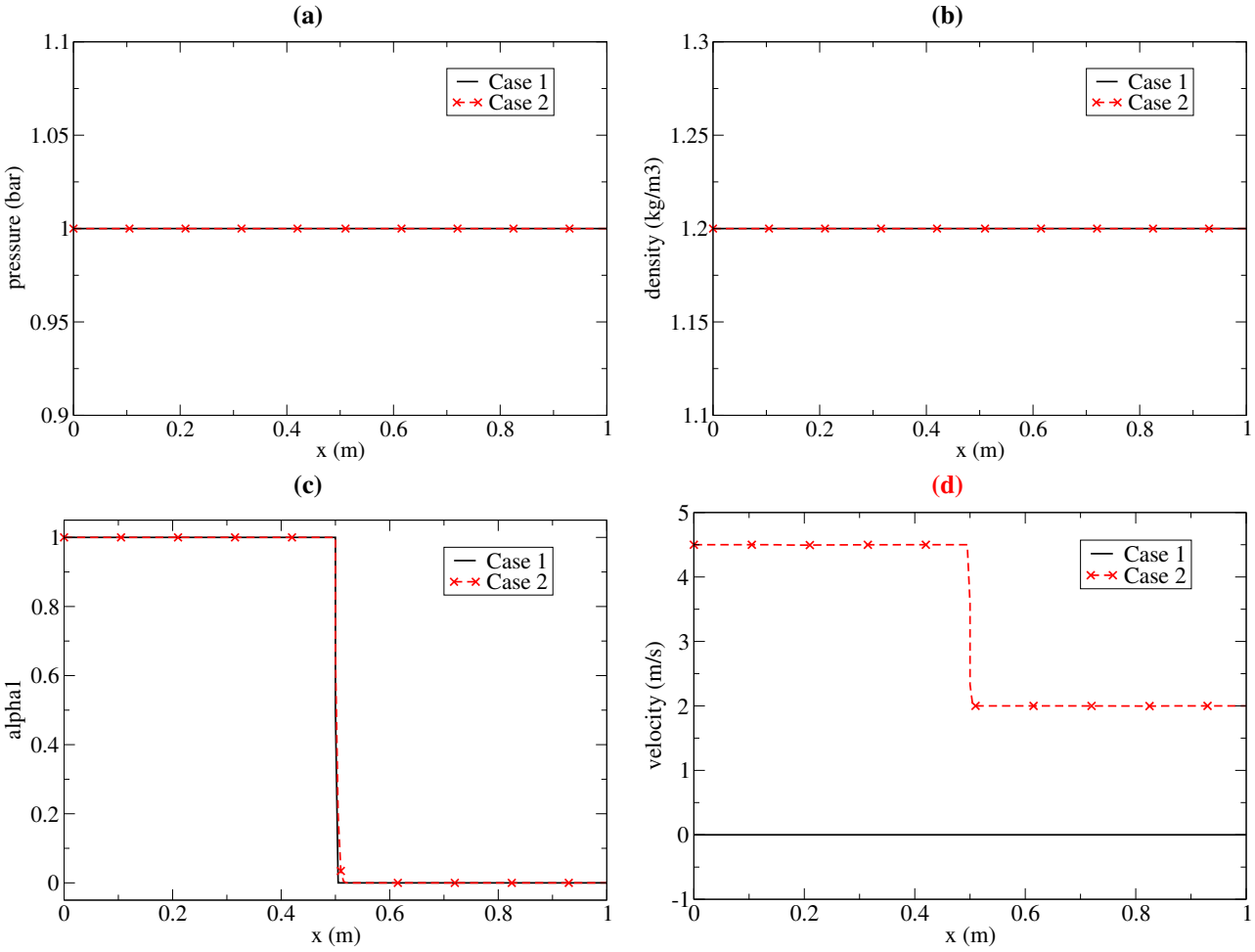

Figure 5: Test 1: Numerical solutions obtained on the well-balanced Riemann problems at $t = 10^{-3}$ s with 200 cells and the Courant number $C = 0.99$: **(a)** mean pressure $p = \alpha_1 p_1 + \alpha_2 p_2$, **(b)** mean density $\rho = \alpha_1 \rho_1 + \alpha_2 \rho_2$, **(c)** volume fraction of phase 1 and **(d)** mean velocity $u = (\alpha_1 \rho_1 u_1 + \alpha_2 \rho_2 u_2)/\rho$.

3.2. Test 2: general Riemann problem in the subsonic configuration on unsplit and split pipe

The second test-case was previously presented in [36] and is largely encountered in the literature [36, 37, 38, 56, 57, 39]. This corresponds to a classical general Riemann problem of the Baer-Nunziato model which involves perfect and stiffened gases. The flow variables in this test-case are assumed to be dimensionless and appropriately normalized. The parameters of the EOS are: $\gamma_1 = 1.35$, $\pi_1 = 0$, $q_1 = 0$, $\gamma_2 = 3$, $\pi_2 = 3400$, $q_2 = 0$ and the initial conditions are given in Table (2). The exact solution of this Riemann problem is composed by 6 waves in the

Position	α_1	p_1	ρ_1	u_1	p_2	ρ_2	u_2	d
$x \in [0; 0.5]$	0.8	3	2	0	10	1900	0	$3\sqrt{2}\|h\|$
$x \in [0.5; 1]$	0.1	1	1	0	1000	1950	0	

Table 2: Dimensionless initial conditions for the general Riemann problem in the subsonic configuration.

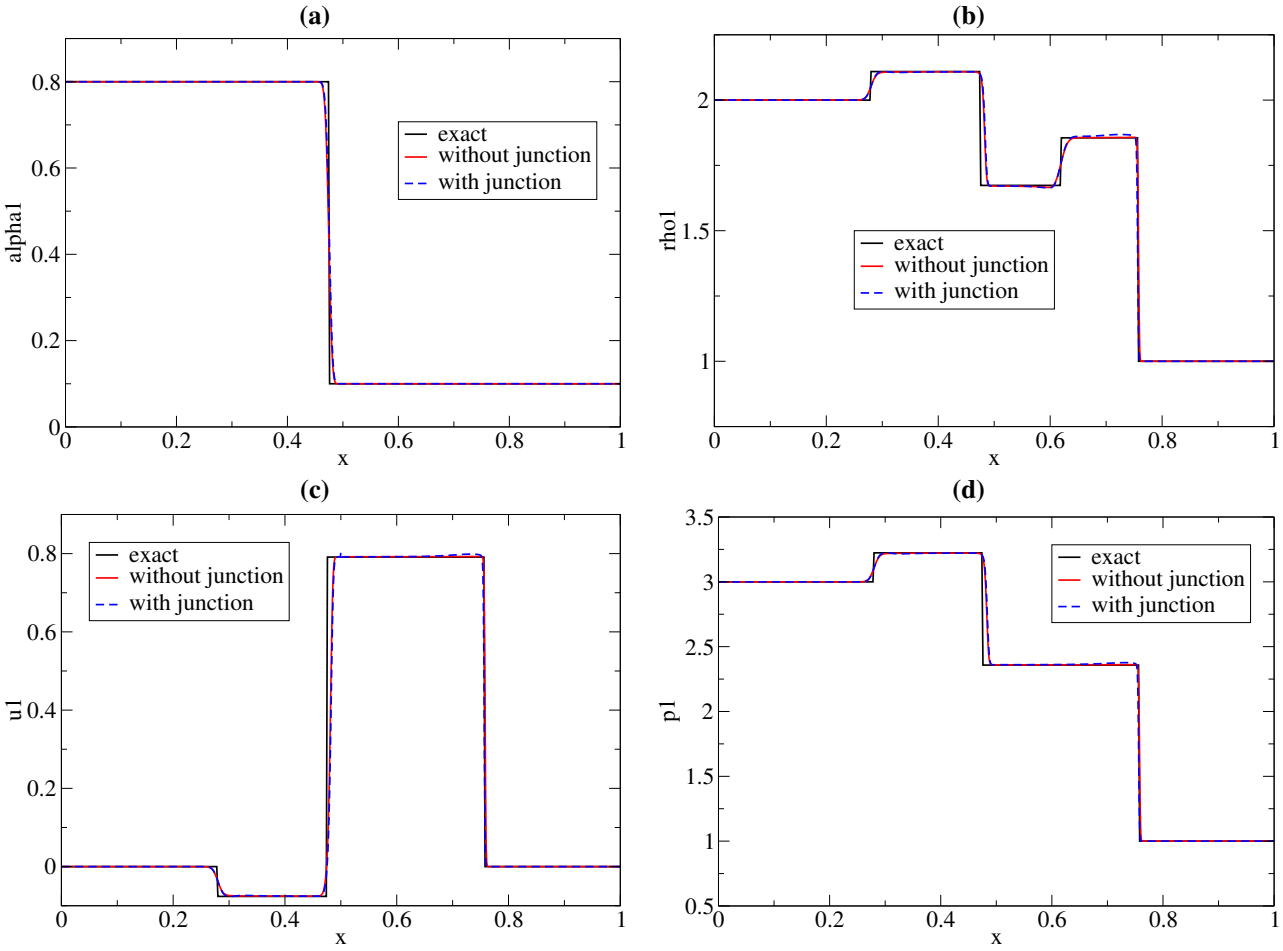

Figure 6: Test 2: Comparison between analytical and numerical solutions for the general Riemann problem in the subsonic configuration with 1000 cells and the Courant number $C = 0.99$: **(a)** volume fraction, **(b)** density, **(c)** velocity and **(d)** pressure of the gaseous phase at $t = 0.15$.

following arrangement: a liquid (phase 2) shock wave, a gas (phase 1) shock wave, the liquid contact, a gas contact, the gas shock wave and finally a liquid rarefaction wave. The computational domain is $[0, 1]$ with a rigid pipe and transmissive boundary conditions are used at the inlet and outlet of the pipe. As in [23, 1], the numerical results using

one single pipe are compared with the ones obtained with two half pipes connected by a junction. The comparison is also performed with the analytical solution of the considered Riemann problem on one single pipe (see Figs (6)-(7)). As in [1], in the case of split pipe, the volume of the fictitious junction cell is set to be equal to the volume of the neighbouring cells leading to $d = 3\sqrt{2}|h|$. The unsplit pipe and split pipe computations are performed with 1000 cells and the Courant number $C = 0.99$. Good agreement is obtained between these two computations which also retrieve the exact solution. However, note that the split pipe computation gives a small oscillation in the post-shock region for the gaseous phase (phase 1) at $x \approx 0.7$.

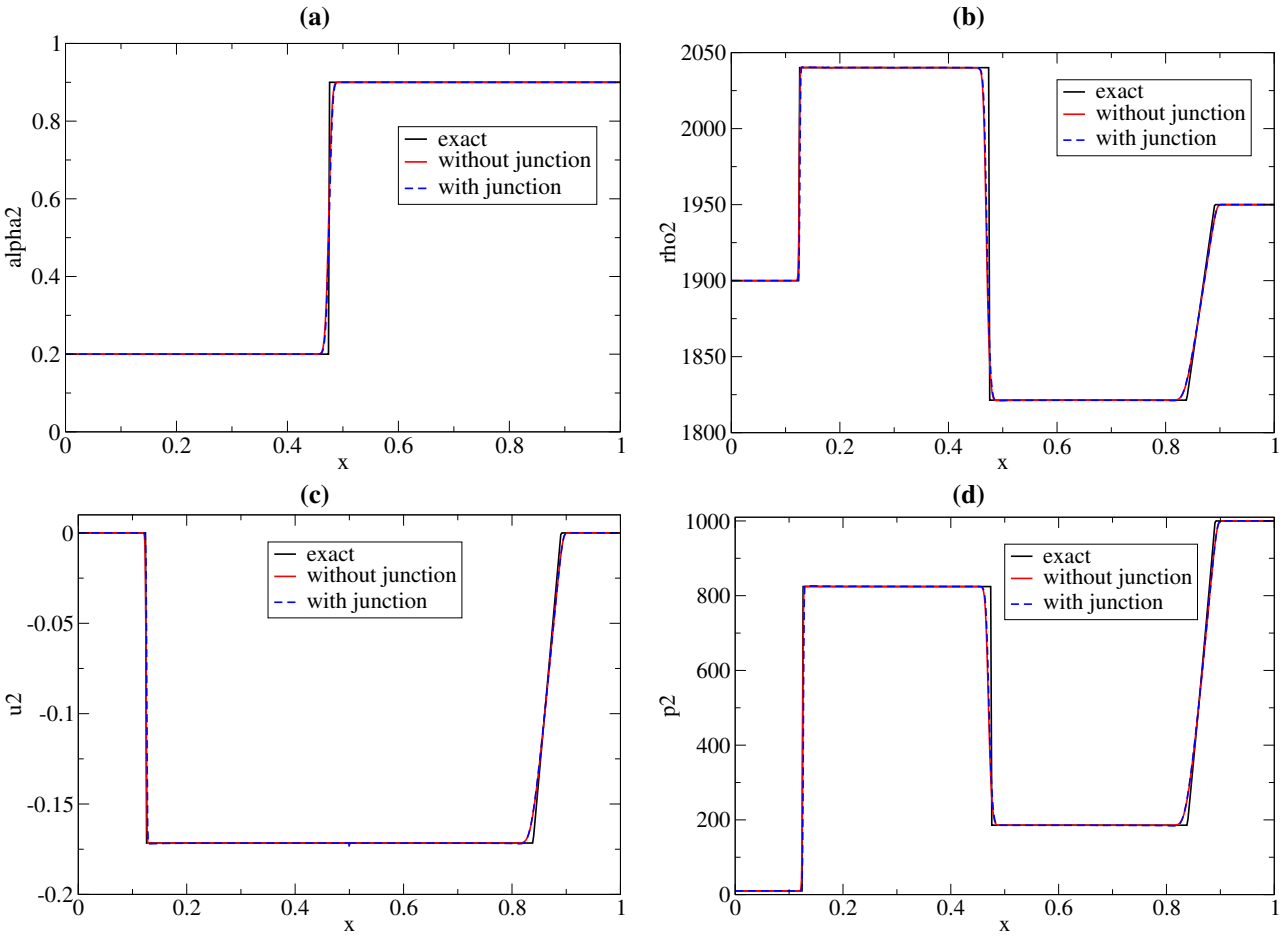

Figure 7: Test 2: Comparison between analytical and numerical solutions for the general Riemann problem in the subsonic configuration with 1000 cells and the Courant number $C = 0.99$: **(a)** volume fraction, **(b)** density, **(c)** velocity and **(d)** pressure of the liquid phase at $t = 0.15$.

3.3. Test 3: general Riemann problem in the supersonic configuration on unsplit and split pipe

This test-case previously proposed in [58] is also used in [39]. Its consists in a general Riemann problem in the supersonic configuration involving two perfect gases. As in the previous case, the flow variables are here assumed to be dimensionless. The parameters of the phasic EOS are: $\gamma_1 = 1.4$, $\pi_1 = 0$, $q_1 = 0$, $\gamma_2 = 1.6$, $\pi_2 = 0$, $q_2 = 0$ and the initial condition is given in Table (3). The exact solution of this Riemann problem is composed by the following waves: a gas (phase1) shock-wave, a gas contact, a gas rarefaction wave, a liquid (phase 2) shock-wave, followed by the liquid contact and a liquid rarefaction wave. The computational domain is [0, 1] with a rigid pipe and transmissive boundary conditions are used at the inlet and outlet of the pipe. Once again, the numerical results obtained using one single pipe are compared to the ones obtained with two half pipes connected by a junction and to the analytical solution

Position	α_1	p_1	ρ_1	u_1	p_2	ρ_2	u_2	d
$x \in [0; 0.5]$	0.5	0.3	0.08545023	−4.7689572	1.8	0.93630573	0.21664237	$3\sqrt{2}\lvert h\rvert$
$x \in [0.5; 1]$	0.55	0.83622836	0.17601423	−5.1681691	2.3327532	1.1009669	0.20870557	

Table 3: Dimensionless initial conditions for the general Riemann problem in the supersonic configuration.

(see Figs (8)-(9)). The unsplit pipe and split pipe computations are performed with 1000 cells and the Courant number $C = 0.99$. For this supersonic Riemann problem, the correction detailed in Eq. (23) is not used for the junction cell. Even in the supersonic configuration, good agreement is obtained between the unsplit pipe and split pipe computations showing the satisfactory behavior of the finite-volume treatment of the junction. Note that an extremely sharp profile

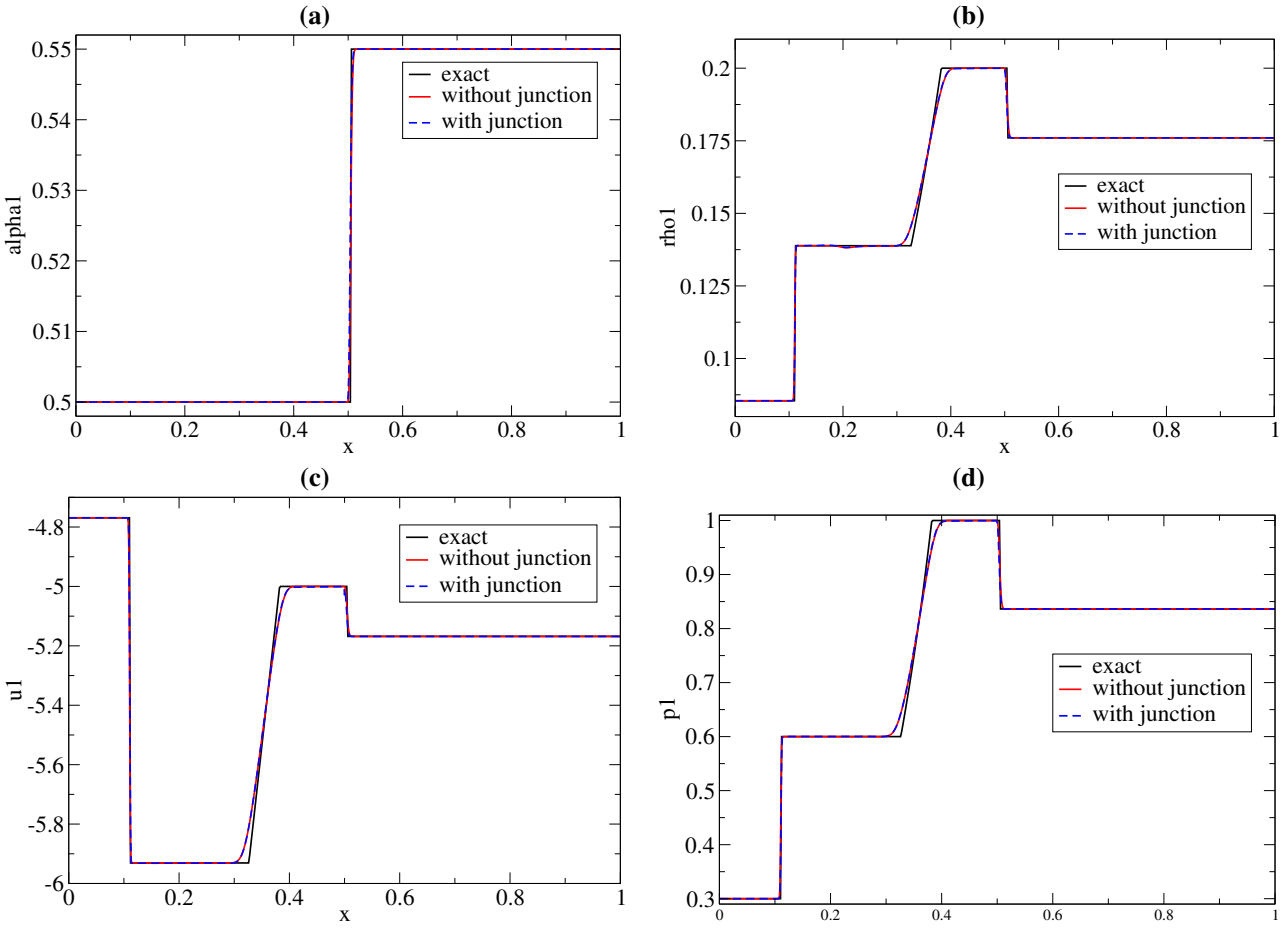

Figure 8: Test 3: Comparison between analytical and numerical solutions for the general Riemann problem in the supersonic configuration with 1000 cells and the Courant number $C = 0.99$: **(a)** volume fraction, **(b)** density, **(c)** velocity and **(d)** pressure of the first phase at $t = 0.05$.

of the liquid contact is obtained even with the use of a junction in the middle of the pipe.

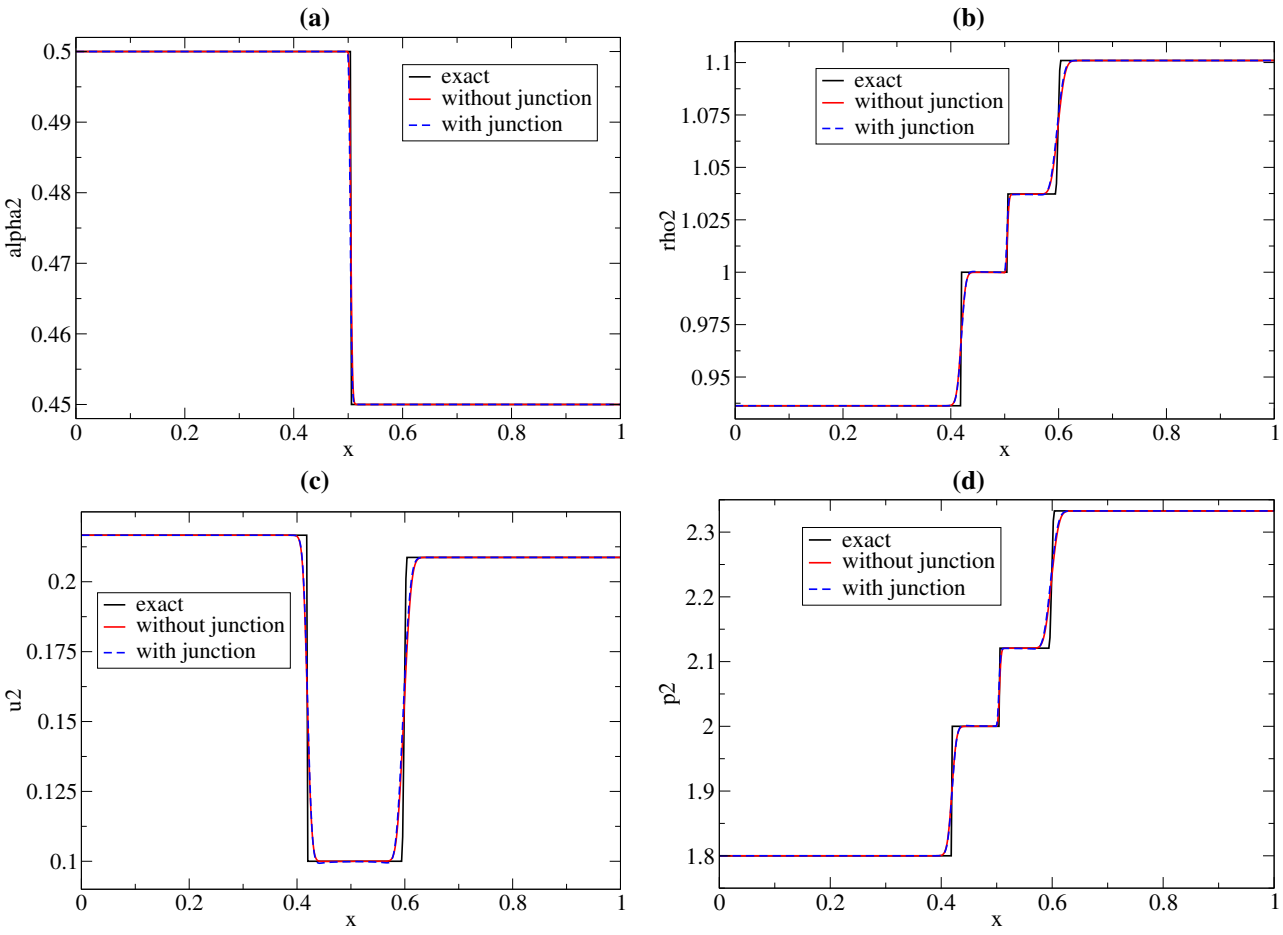

Figure 9: Test 3: Comparison between analytical and numerical solutions for the general Riemann problem in the supersonic configuration with 1000 cells and the Courant number $C = 0.99$: **(a)** volume fraction, **(b)** density, **(c)** velocity and **(d)** pressure of the second phase at $t = 0.05$.

3.4. Test 4: Shock wave interaction with a sudden cross-section reduction in a duct

This test-case was first proposed in [5] and also used in [59, 1]. The initial conditions are given in Table (4) using two perfect gases with $\gamma_1 = \gamma_2 = 1.4$. This test consists in a 2-m long rigid tube filled by a gas at rest. A sudden

Position	α_1	p_1 (Pa)	ρ_1 (kg.m^{-3})	u_1 (m.s^{-1})	p_2 (Pa)	ρ_2 (kg.m^{-3})	u_2 (m.s^{-1})	d (m)
$x \in [0; 0.7]$	0.8	30×10^5	35.6	0	30×10^5	35.6	0	0.1
$x \in [0.7; 1.4]$	0.8	10^5	1.1867	0	10^5	1.1867	0	0.1
$x \in [1.4; 2]$	0.8	10^5	1.1867	0	10^5	1.1867	0	0.06324

Table 4: Initial conditions for the gas Riemann problem with an abrupt change of area.

cross-section reduction is located at $x = 1.4$ m and a shock-wave is initially located at $x = 0.7$ m. Transmissive boundary conditions are used at the two boundaries of the tube. The numerical solutions obtained with 1000 cells and the Courant number $C = 0.99$ are compared to two numerical solutions obtained with the Euler equations, one using the quasi 1-D numerical approach of Rochette *et al.* [5] and the other using the numerical treatment proposed in [1]. The volume of the fictitious junction cell is set to be equal to 10^{-5} m^3 which corresponds to the average volume for of the pipe cells at the vicinity of the junction cell. As expected, the numerical extension of the junction is in perfect

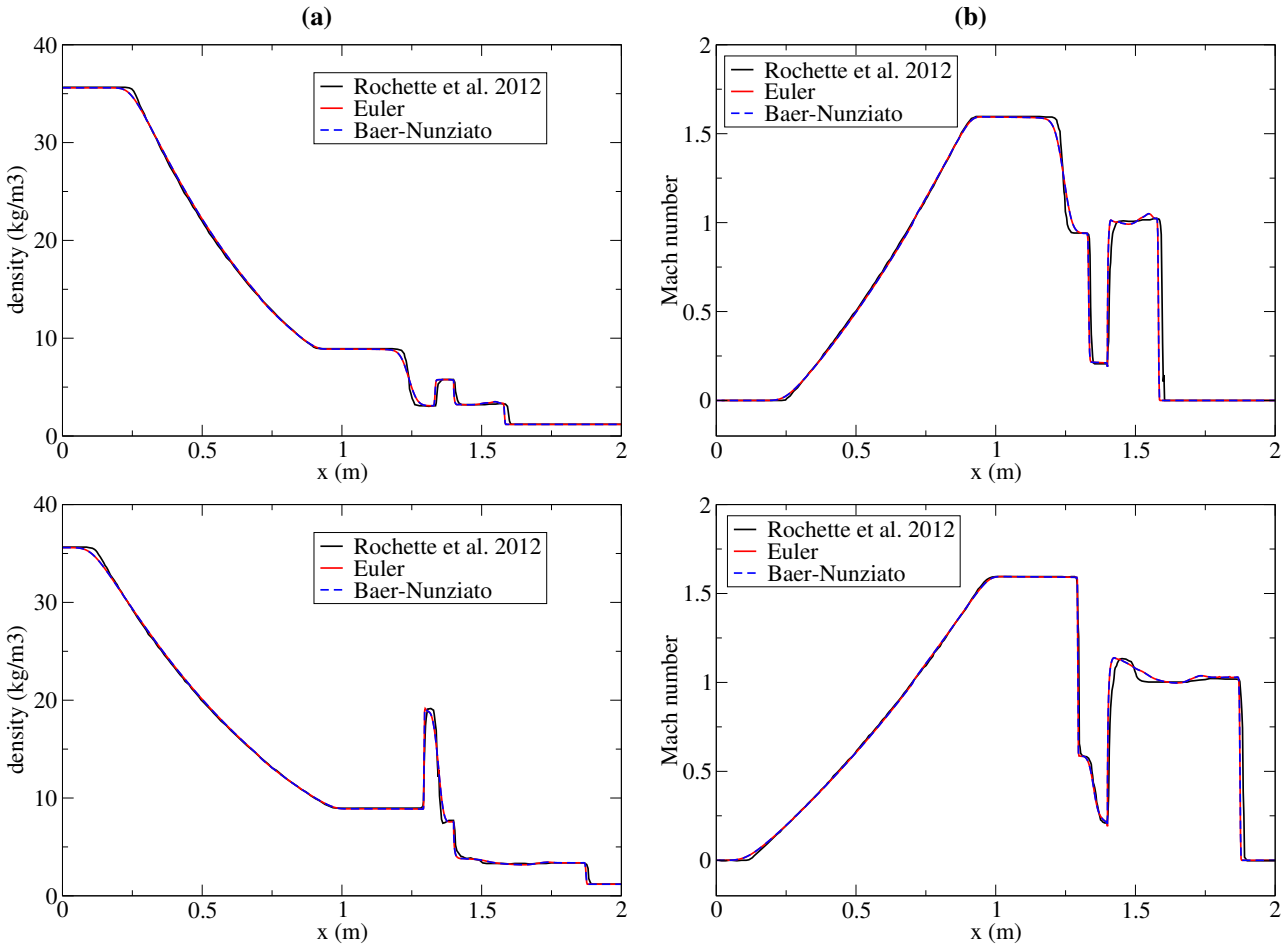

Figure 10: Test 4: Numerical solutions obtained on the gas Riemann problem with the abrupt change of area using 1000 cells and $C = 0.99$ at $t = 1.3 \times 10^{-3}$ s (top) and $t = 1.7 \times 10^{-3}$ s (bottom): **(a)** mean density $\rho = \alpha_1\rho_1 + \alpha_2\rho_2$ and **(b)** phasic Mach number $|u_1|/c_1$.

agreement with the one proposed for the Euler equations (see Fig. (10)). In this test-case, there is no jump of the volume fraction α_1 leading to the degeneration of the Baer-Nunziato model into a decoupled Euler equations. This is also numerically observed here.

3.5. Test 5: Liquid shock-wave interaction with a sudden cross-section reduction in a duct

The single-phase counterpart of this test-case was proposed in [1]. The initial conditions are detailed in Table (5). The parameters of the phasic EOS are: $\gamma_1 = \gamma_2 = 2.25$, $\pi_1 = \pi_2 = 10^9$ Pa and $q_1 = q_2 = 0$ J.kg^{-1}. This consists in a

Position	α_1	p_1 (Pa)	ρ_1 (kg.m^{-3})	u_1 (m.s^{-1})	p_2 (Pa)	ρ_2 (kg.m^{-3})	u_2 (m.s^{-1})	d (m)
$x \in [0;2]$	0.8	10^6	998.638	0	10^6	998.638	0	2×10^{-2}
$x \in [2;3]$	0.3	10^5	998.228	0	10^5	998.228	0	2×10^{-2}
$x \in [3;5]$	0.3	10^5	998.228	0	10^5	998.228	0	1×10^{-2}

Table 5: Initial conditions for the liquid Riemann problem with an abrupt change of area.

5-m long rigid pipe filled by liquid water at rest at temperature $T = 20°C$. A sudden contraction of the cross section

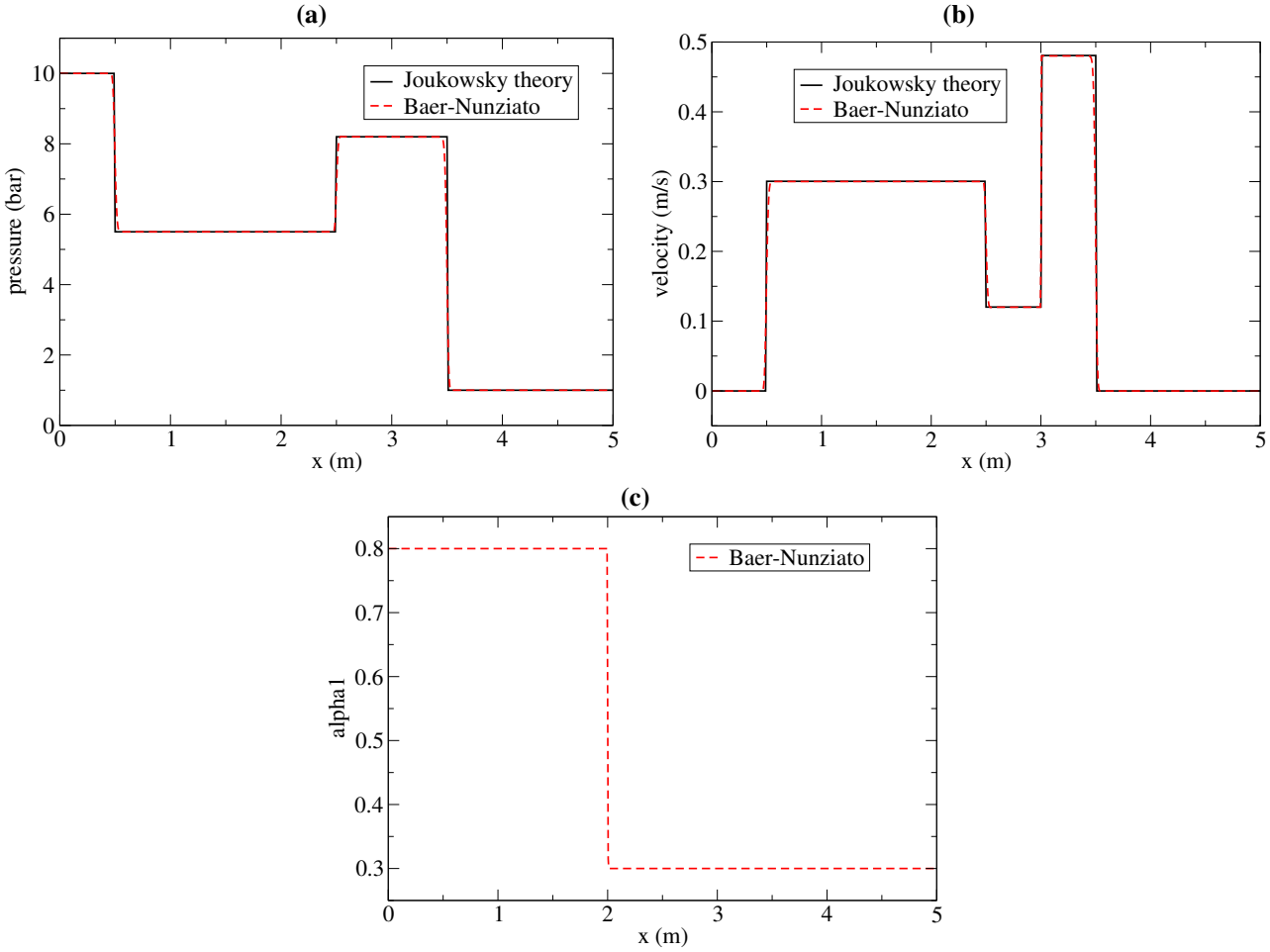

Figure 11: Test 5: Comparison between numerical and Joukowsky-type solutions on the liquid Riemann problem with an abrupt change of area with 1000 cells and $C = 0.99$ at $t = 10^{-3}$ s: **(a)** mean pressure $p = \alpha_1 p_1 + \alpha_2 p_2$, **(b)** phasic velocity u_1 and **(c)** volume fraction of phase 1.

is located at $x = 3$ m and a pressure jump is initially located at $x = 2$ m. The numerical solutions obtained with 1000 cells and a Courant number $C = 0.99$ is compared to the analytical solution obtained with the Joukowsky theory [7, 50]. All of the intermediate states predicted by this theory is well retrieved by the present computation showing the satisfactory behavior of the Finite-Volume junction treatment (see Fig. (11)).

3.6. Test 6: Riemann problem in rigid and elastic pipes

This test-case is similar to the one proposed in [1] in the single-phase context. The parameters of the phasic EOS are the following: $\gamma_1 = \gamma_2 = 2.25$, $\pi_1 = \pi_2 = 10^9$ Pa and $q_1 = q_2 = 0$ J.kg^{-1}. The initial conditions and the material conditions used to represent the elastic behavior of the pipe are given in Table (6). A 1-m long tube is

(a)

Position	α_1	p_1 (Pa)	ρ_1 (kg.m^{-3})	u_1 (m.s^{-1})	p_2 (Pa)	ρ_2 (kg.m^{-3})	u_2 (m.s^{-1})
$x \in [0; 0.5]$	0.8	10^6	998.638	0	10^6	998.638	0
$x \in [0.5; 1]$	0.3	10^5	998.228	0	10^5	998.228	0

(b)

d (m)	δ (m)	E (MPa)	ν_P
19×10^{-3}	1.6×10^{-3}	75×10^3	0.3

Table 6: Initial conditions **(a)** and wall material properties **(b)** for the Riemann problem in rigid and elastic pipes.

considered with transmissive boundary conditions are used at the inlet and outlet. The initial discontinuity is located at $x = 0.5$ m. The Riemann problem is solved using rigid and then elastic pipes taking into account the variation of

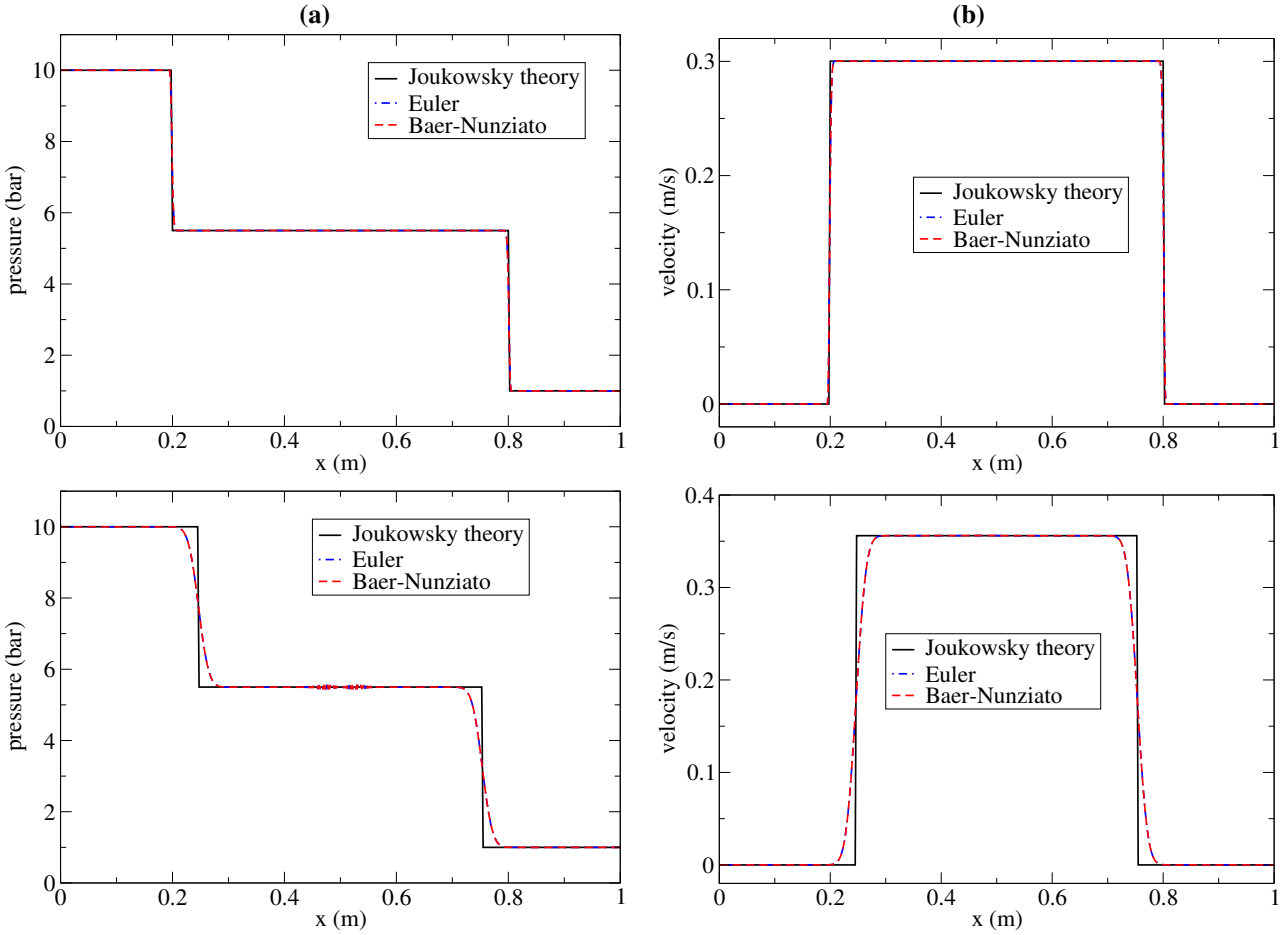

Figure 12: Test 6: Comparison between numerical and Joukowsky-type solutions on the Riemann problem in rigid (top) and elastic (bottom) pipes at $t = 2 \times 10^{-4}$ s with 800 cells: **(a)** mean pressure $p = \alpha_1 p_1 + \alpha_2 p_2$ and **(b)** phasic velocity u_1.

the pipe cross-section due to the change of pressure as described previously. The numerical solutions obtained with the Baer-Nunziato model are compared to the ones obtained with the Euler system in conjunction of the SG EOS with the parameters given previously. These two numerical results are also in agreement with the theoretical results obtained with the classical Joukowsky-Allievi theory (see Figs. (12,13)). The computations are done with 800 cells. The computation with the rigid pipe uses a Courant number $C = 0.99$ whereas the one with the elastic pipe is stable for a Courant number $C = 0.6$. The same behavior is also observed with the Euler equations. Notice that some spurious

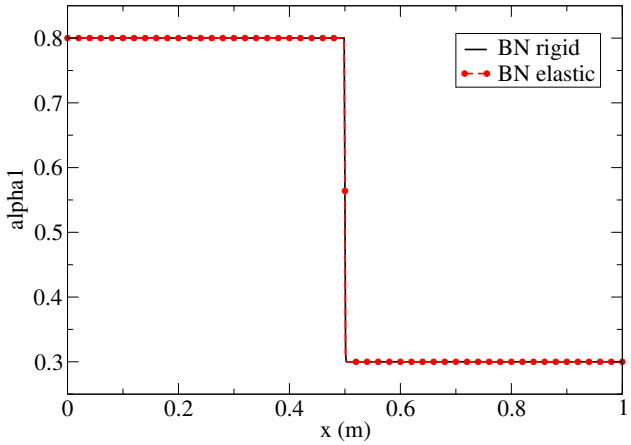

Figure 13: Test 6: Volume fraction of phase 1 on the Riemann problem in rigid and elastic pipes at $t = 2 \times 10^{-4}$ s with 800 cells.

oscillations are visible at $x = 0.5$ m on the pressure profiles in both Baer-Nunziato and Euler solutions obtained with the elastic pipe. These oscillations can be reduced with a decrease of the Courant number.

3.7. Test 7: Water-hammer experiment with vapor cavity formation and collapse

The present test-case is one of the experiments conducted by Simpson [60, 61] in order to study the generation of cavitation during a water-hammer event. The present experimental set-up is here modeled using an ideal tank-pipe-valve system without FSI junction coupling. The pressure wave is initiated by the sudden closure of the valve. After wave reflection cavitation occurs at the valve and vapor appears. The generated vapor then condenses with the collapsing vapor region creating a second pressure wave interacting with the first one. The initial conditions for the fluid and the material properties for the pipe wall used in the computation are given in Table (7) as well as the parameters of the phasic EOS. The present computations have been performed using 1000 cells and the Courant

(a)

α_1	p_1 (Pa)	ρ_1 (kg.m^{-3})	u_1 (m.s^{-1})	p_2 (Pa)	ρ_2 (kg.m^{-3})	u_2 (m.s^{-1})
10^{-6}	3.281×10^5	2.53	0.401	3.281×10^5	997.9	0.401

(b)

L (m)	d (m)	δ (m)	E (MPa)	ν_P
36.0	19×10^{-3}	1.6×10^{-3}	75×10^3	0.3

(c)

γ_1	π_1 (Pa)	q_1 (J.kg^{-1})	γ_2	π_2 (Pa)	q_2 (J.kg^{-1})
1.34	0	2009800	2.79	7.9442566335×10^8	-1142331

Table 7: Flow initial conditions **(a)**, wall material properties **(b)** and parameters of the phasic EOS **(c)** for the Simpson's pipe column-separation water-hammer experiment.

number $C = 0.6$ in Eq. (19). In contrast to the other cases, the Rusanov flux is here used for a stability reason. The velocity and pressure relaxation terms [43] are also used in the present computation. More details on the relaxation process are given in Appendix A. In addition, the pipe wall hoop elasticity is also considered as detailed in Section 2.1.7. The closure of the valve is here assumed to be instantaneous and thus modeled by a wall boundary condition. The initial speed of sound is given by:

$$c_0 = c_2 \equiv \sqrt{\frac{\gamma_2 \left(p_2 + \pi_2\right)}{\rho_2}}$$

leading to the numerical value: $c_0 \approx 1490$ m.s^{-1}. Using the Korteweg formula [52] for the effective speed of sound:

$$\tilde{c}_0^2 = \frac{c_0^2}{1 + \dfrac{\rho_0 \beta c_0^2}{E}} \quad \text{where} \quad \beta = \frac{2}{\left[(d+2\delta)^2 - d^2\right]} \left[(1-\nu_P)\, d^2 + (1+\nu_P)\,(d+2\delta)^2\right]$$

with $\rho_0 = \rho_2$ leads to the following value: $\tilde{c}_0 = 1259$ m.s^{-1} which corresponds with an error of 1.6% to the measurement of Simpson: $\tilde{c}_{\text{exp.}} = 1280$ m.s^{-1}. Fig. (14) represents the comparison between the experimental data obtained by Simpson and the present numerical results for the pressure histories at three different locations along the pipe: at the valve ($x = L$), at $x = 3L/4$ and at $x = L/4$. Good agreement is obtained. In particular, the magnitude of the first pressure peak given by the classical Joukowsky relation $p_{\max} = p_0 + \rho_0 \tilde{c}_0 u_0 \approx 8.318$ bar is observed in the computation. Then, the reflection of the rarefaction wave at the valve at $t = 2L/\tilde{c}_0 \approx 57$ ms induces cavitation and thus a generation of vapor. Afterwards, the vapor collapses at the valve at $t \approx 135$ ms generating a second pressure wave. The interaction between the first and the second pressure peaks leads to the highest magnitude at the valve at $t = 6L/\tilde{c}_0 \approx 171$ ms.

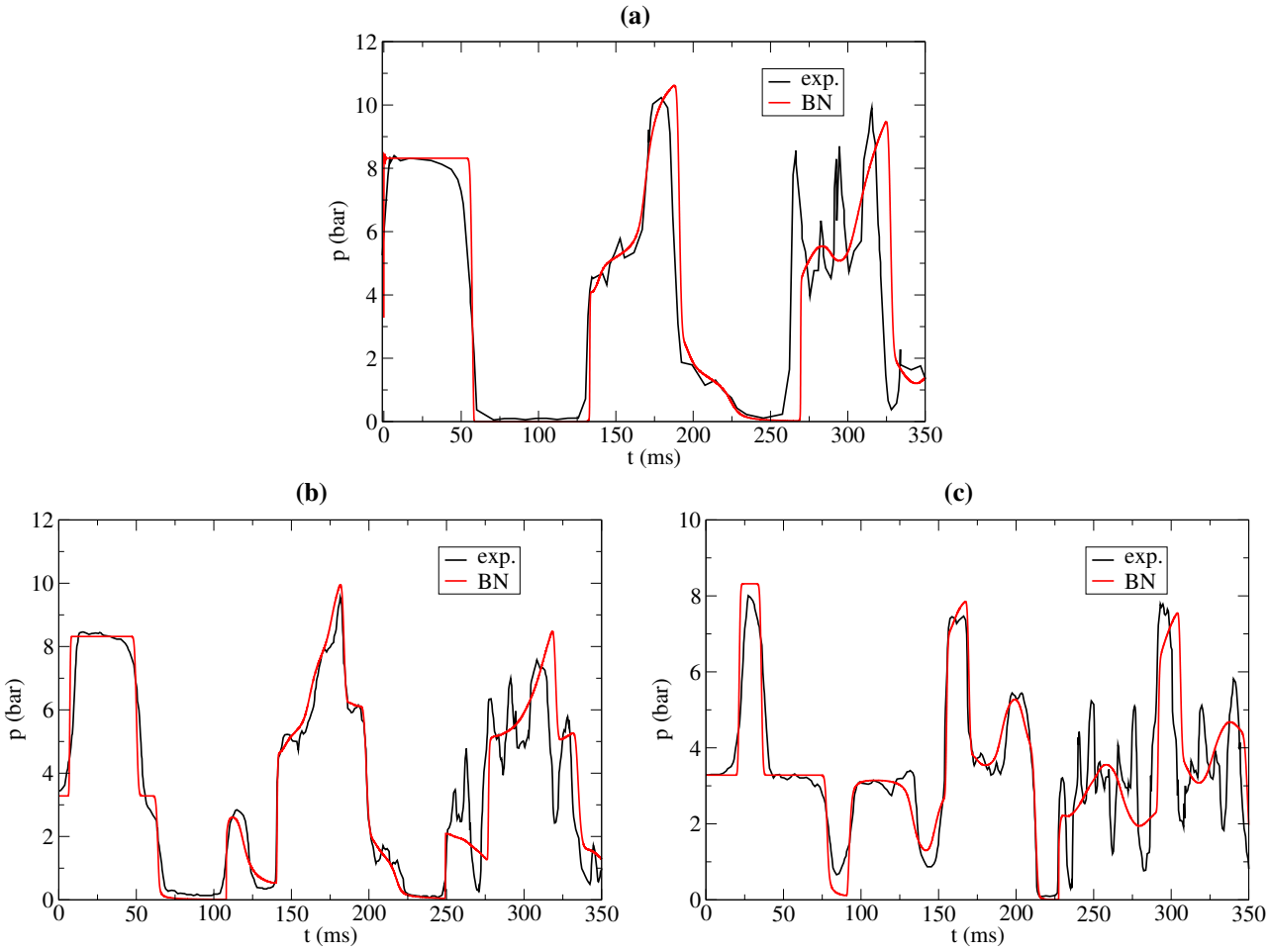

Figure 14: Test 7: Comparison between numerical solutions obtained with 1000 cells and $C = 0.6$ and the data of Simpson's water-hammer experiment with $u_0 = 0.401$ m.s^{-1}: pressure history **(a)** at $x = L$ (valve); **(b)** at $x = 3L/4$; **(c)** at $x = L/4$.

3.8. Test 8: Hydraulic shock wave in a three-pipe network

This test initially proposed in Tiselj *et al.* [62, 63] and also used in [1] consists in the propagation of a pressure wave through a junction of three rigid pipes filled with pure liquid. The initial conditions and the geometrical data

Position	α_1	p_1 (Pa)	ρ_1 (kg.m^{-3})	u_1 (m.s^{-1})	p_2 (Pa)	ρ_2 (kg.m^{-3})	u_2 (m.s^{-1})	d (m)	l (m)
Pipe 1	0.8	80×10^5	1001.89	1	80×10^5	1001.89	1	0.35682482	10
Pipe 2	0.1	80×10^5	1001.89	0.769	80×10^5	1001.89	0.769	0.19544100	3
Pipe 3	0.6	80×10^5	1001.89	0.769	80×10^5	1001.89	0.769	0.35682482	5

Table 8: Initial conditions of the three-pipe problem.

(diameter d and length l) of each pipes are given in Table (8). The parameters of the phasic EOS are the following:

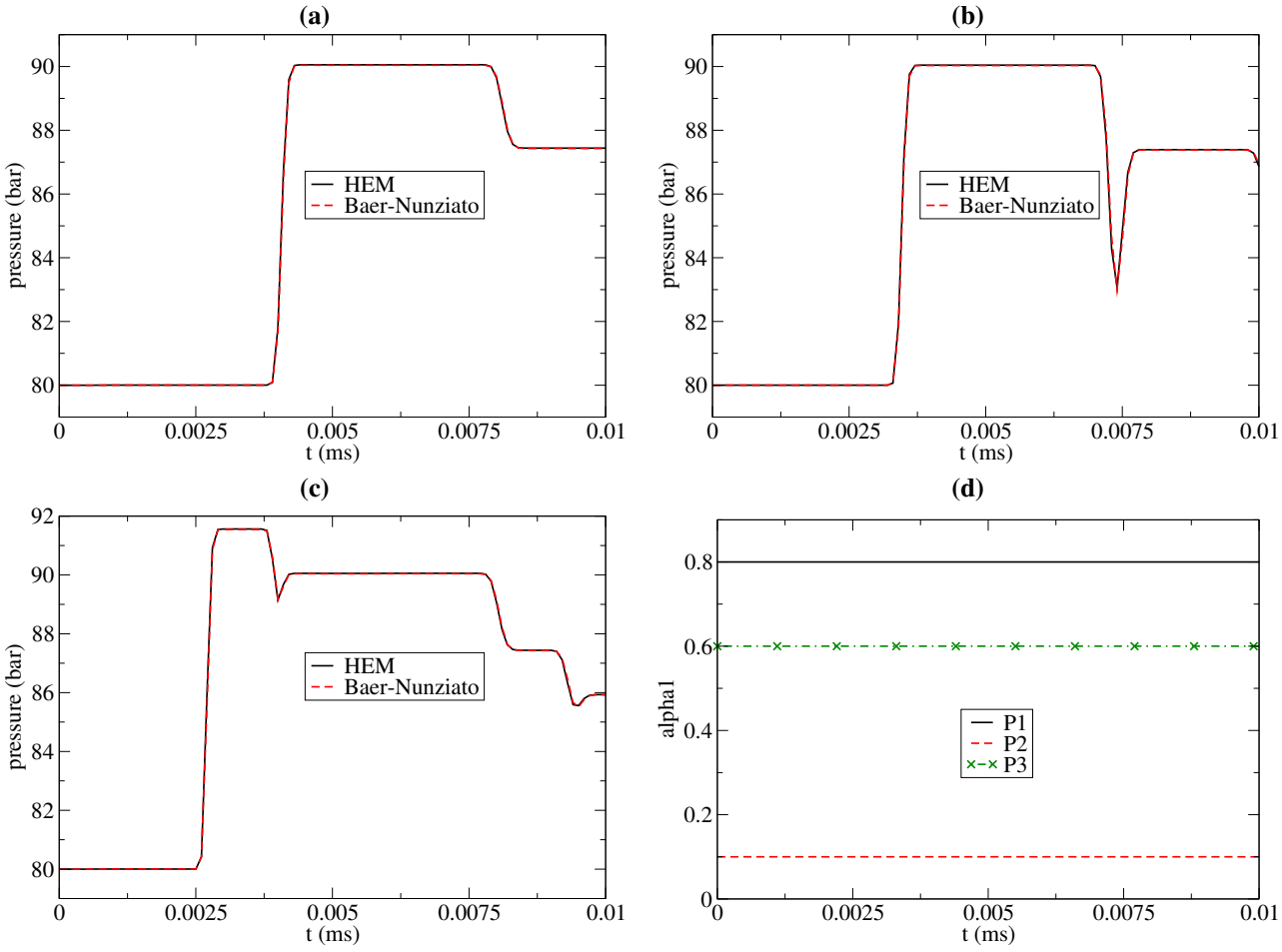

Figure 15: Test 8: Numerical solutions obtained on the junction problem of three pipes with $h = 10^{-2}$ m and $C = 0.8$: time evolution of the mean pressure $p = \alpha_1 p_1 + \alpha_2 p_2$ at **(a)** point 1, **(b)** point 2, **(c)** point 3, and **(d)** time evolution of the volume fraction α_1 in the three pipes, comparison with HEM.

$\gamma_1 = \gamma_2 = 2.23$, $\pi_1 = \pi_2 = 10^9$ Pa and $q_1 = q_2 = 0$ J.kg^{-1}. The inlet condition of Pipe 1 and the outlet condition of Pipe 2 correspond to a tank condition using the volume $|C_{\text{tank}}| = 10^5$ m^3, the pressure $p_{\text{tank}} = 80$ bar and the density $\rho_{\text{tank}} = 1001.89$ kg.m^{-3} (which corresponds to the temperature $T_{\text{tank}} = 19.85°C$) whereas the outlet condition of Pipe 3

is a wall condition in order to represent the sudden closure of the end of Pipe 3. Due to this sudden closure, a pressure wave is created and propagates through the three-pipe network. The computations obtained with the Baer-Nunziato model are compared to the ones using the HEM model in conjunction with the NBS/NRC Steam Tables [64] presented in [1] with a grid size $|h| = 10^{-2}$ m and a Courant number $C = 0.8$. The corresponding history of pressure in point 1 (located at 1.05 m from the junction in Pipe 1), in point 2 (located at 0.15 m from the junction in Pipe 2) and in point 3 (located at 0.95 m from the junction in Pipe 3) are displayed in Fig. (15). Very good agreement between HEM and Baer-Nunziato are obtained. In addition, the Finite-Volume treatment of junctions handles the jump of volume fraction quite satisfactorily.

3.9. Shock-tube experiments in a network connected by a junction

The experiments conducted by William-Louis *et al.* [65] are here considered to assess the present Finite-Volume treatment of junctions in the framework of the Baer-Nunziato model. Three configurations are studied in this section. The first one is composed by three pipes while the second and the third ones are composed by four pipes. In all cases,

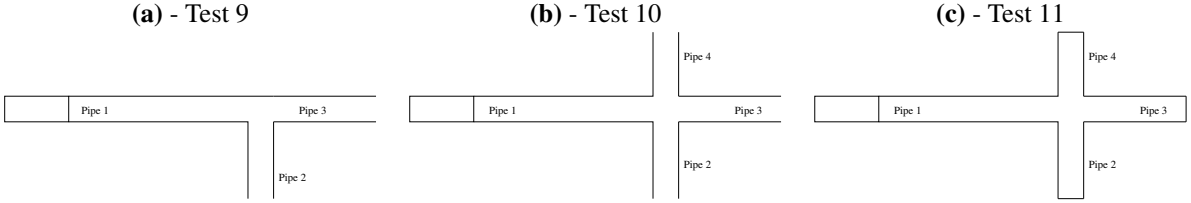

Figure 16: Sketch of William-Louis *et al.*'s experimental apparatus from [65]: **(a)** with three open end branches, **(b)** with four open end branches and **(c)** with four closed end branches.

the first pipe consists of a shock-tube with a high-pressure chamber of length 0.53 m and a low-pressure chamber of length 3.1 m connected to the (two or three) other pipes by a junction. The different configurations are represented

	Pipe 1 (HP)	Pipe 1 (LP)	Pipe 2 (LP)	Pipe 3 (LP)	Pipe 4 (LP)
l (m)	0.53	3.1	2.595	1.725	0.845
d (m)	0.01				

Table 9: Geometrical data (length and internal diameter) for the three William-Louis *et al.*'s experiments [65].

in Fig. (16) and the corresponding geometrical data are given in Table (9) where the initial HP and LP denote the high-pressure and low-pressure states, respectively. The three or four pipes have the same inner diameter of $d = 0.01$ m in the present computations. Finally, the HP and LP states characterized by a pressure difference of $\Delta p = 15$ kPa are recalled in Table (10). The experimental pressure measurements performed by William-Louis *et al.* [65] are

Position	α_1	p_1 (Pa)	ρ_1 (kg.m^{-3})	u_1 (m.s^{-1})	p_2 (Pa)	ρ_2 (kg.m^{-3})	u_2 (m.s^{-1})
High-pressure	$1 - 10^{-6}$	1.15×10^5	1.4145	0	10^5	1.23	0
Low-pressure	10^{-6}	1.15×10^5	1.4145	0	10^5	1.23	0

Table 10: Initial conditions of the shock-tube connected by other pipes by a junction [65].

conducted far enough from the junction to ensure that the waves are planar at the locations of the pressure transducers (about $x \approx 0.5$ m from the junction in each pipe). All of the computations are performed using a constant space step $h_i = 1/3$ m and Courant number $C = 0.95$. The corresponding numerical solutions are then compared to the experimental data. This comparison is based on the numerical mean pressure defined as $p = \alpha_1 p_1 + \alpha_2 p_2$.

3.9.1. Test 9: Shock-wave propagation in a three-pipe network

This test-case composed by three pipes connected at a junction is represented in Fig. (16)-**(a)** and the corresponding initial conditions are detailed in Table (10). The ends of the three pipes are considered to be open and are thus modeled using a "tank" condition in the present computations as given in Eq. (28). The prescribed phasic volume fractions, densities and pressures correspond to the initial conditions, i.e. the HP state for the end of Pipe 1 and the LP state for the ends of Pipe 2 and Pipe 3. The prescribed "tank" volume is set equal to $|C_{\text{tank}}| = 10^9$ m^3 which is large enough to ensure that the "tank" conditions are constant during the simulation. The comparison between the

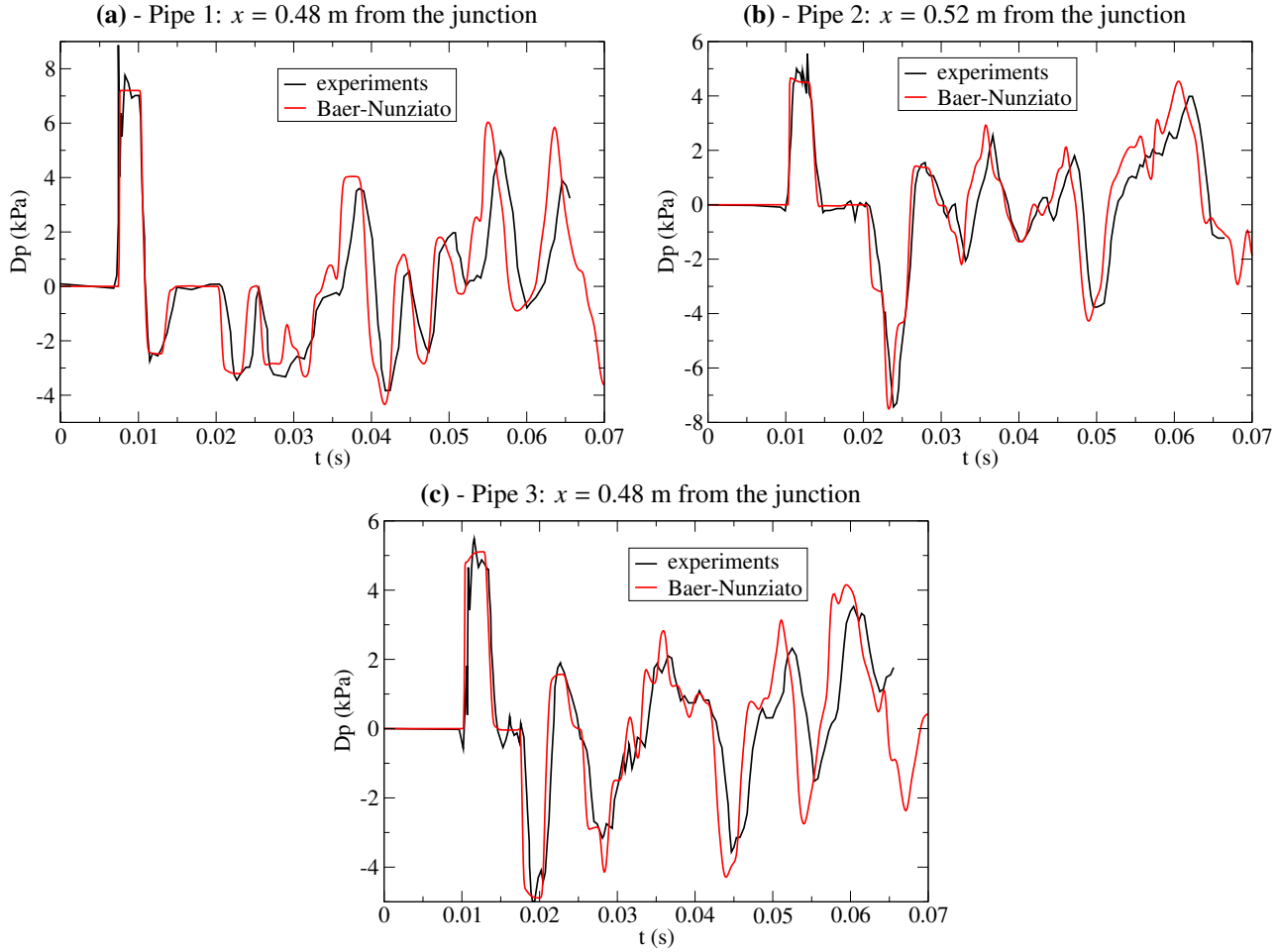

Figure 17: Test 9: Comparison between the numerical solutions of the Baer-Nunziato model obtained with $h = 1/3$ cm, $C = 0.95$ and the data of William-Louis *et al.*'s shock-tube experiment with three pipes and *open ends*: pressure history **(a)** in Pipe 1 at $x = 0.48$ m from the junction, **(b)** in Pipe 2 at $x = 0.52$ m from the junction and **(c)** in Pipe 3 at $x = 0.48$ m from the junction.

numerical solutions of the Baer-Nunziato model and the experimental data from [65] is given in Fig. (17) for the three pipes. The pressure histories show the interactions occurring between the different pressure waves and the junction. First, the initial pressure wave induced by the shock-tube interacts with the junction leading to a reflected pressure wave propagating in Pipe 1 and two transmitted pressure waves propagating in Pipe 2 and Pipe 3. These pressure waves reach the ends of each pipe leading to reflections where the corresponding prescribed pressures are imposed: $p = 1.15$ bar for Pipe 1 and $p = 1$ bar for Pipe 2 and Pipe 3. Subsequently, other interactions with the junction occur. The good agreement between the numerical and the experimental results demonstrates the satisfactory behavior of the Finite-Volume junction modeling proposed for the Baer-Nunziato model: both timing and amplitude of the pressure

waves are well captured in the computation.

3.9.2. Test 10: Shock-wave propagation in a four-pipe network with open ends

The present test-case represented in Fig. (16)-**(b)** corresponds to a four-pipe network with open ends. The length of the four pipes are chosen to be different in order to induce asynchronous timings between the secondary pressure waves generated by the reflection at the ends of the pipes. Once again the initial conditions are given in Table (10) while the open ends are modeled with "tank" conditions (see Eq. (28)) as detailed in the previous test-case. The

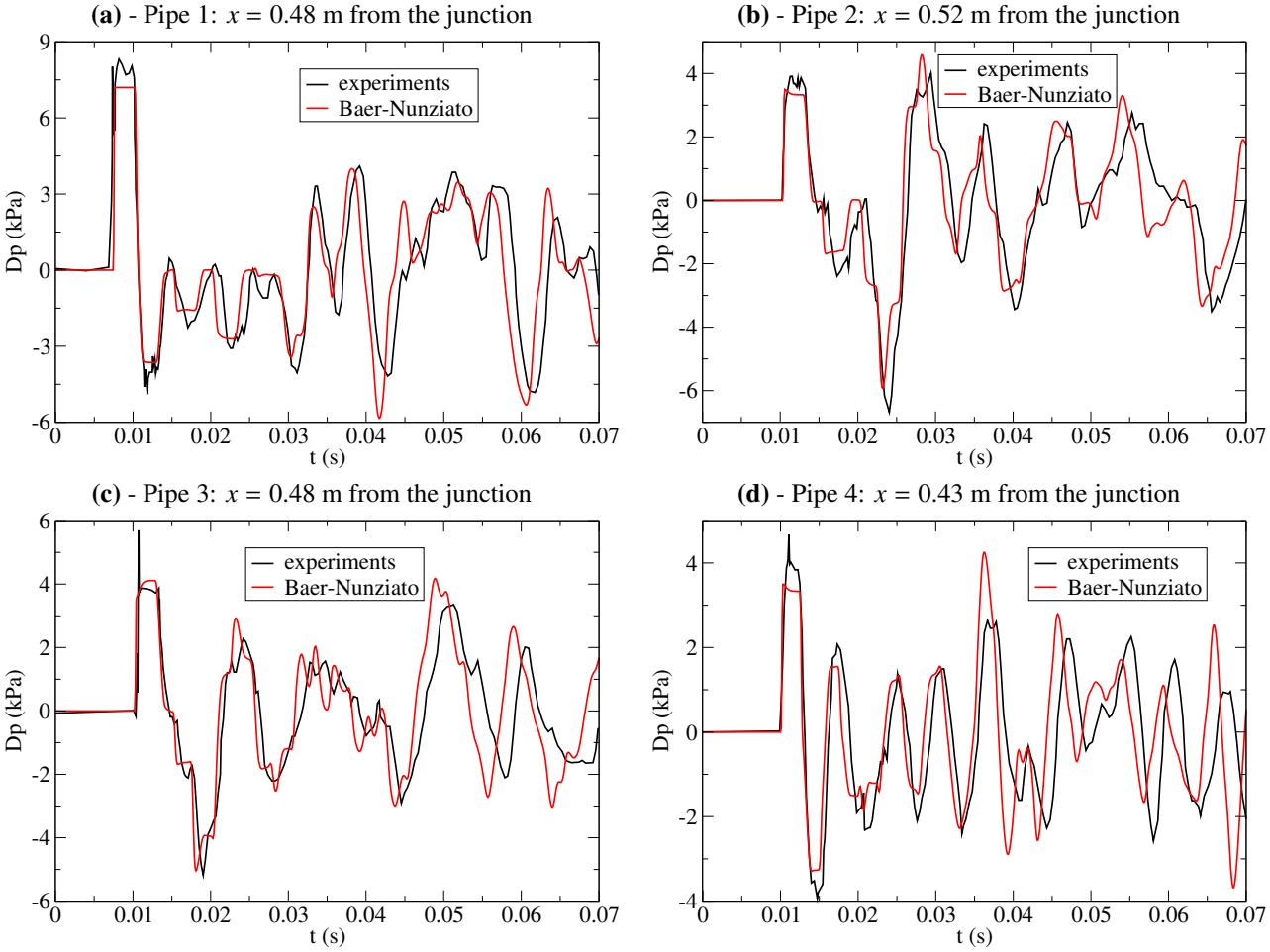

Figure 18: Test 10: Comparison between the numerical solutions of the Baer-Nunziato model obtained with $h = 1/3$ cm, $C = 0.95$ and the data of William-Louis *et al.*'s shock-tube experiment with four pipes and *open ends*: pressure history **(a)** in Pipe 1 at $x = 0.48$ m from the junction, **(b)** in Pipe 2 at $x = 0.52$ m from the junction, **(c)** in Pipe 3 at $x = 0.48$ m from the junction and **(d)** in Pipe 4 at $x = 0.43$ m from the junction.

numerical solution of the Baer-Nunziato model is then compared with the experimental measurements from William-Louis *et al.* [65]. Even in this complex configuration where numerous interactions between pressure waves and the junction occur, the numerical solution is in good agreement with the reference experimental results.

3.9.3. Test 11: Shock-wave propagation in a four-pipe network with closed ends

This test-case is based on the previous one except that the ends of the four pipes are here closed. The wall boundary condition detailed in Eq. (25) is thus retained to take into account this effect. The comparison between the numerical solutions of the Baer-Nunziato with the experimental data of William-Louis *et al.* [65] is given in Fig. (19). Once again, the present Finite-Volume junction modeling makes it possible to simulate the numerous interactions between

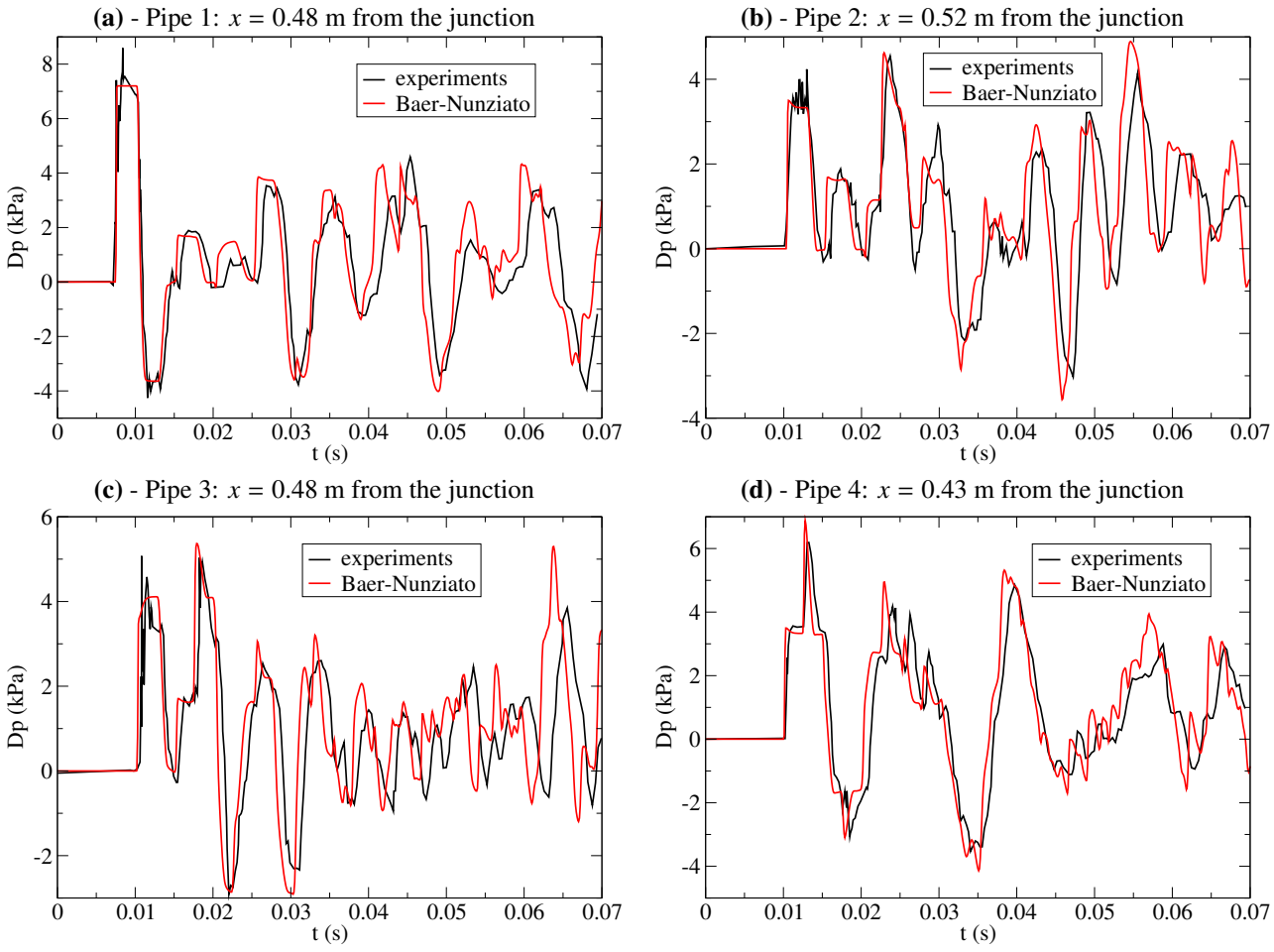

Figure 19: Test 11: Comparison between the numerical solutions of the Baer-Nunziato model obtained with $h = 1/3$ cm, $C = 0.95$ and the data of William-Louis *et al.*'s shock-tube experiment with four pipes and *closed ends*: pressure history **(a)** in Pipe 1 at $x = 0.48$ m from the junction, **(b)** in Pipe 2 at $x = 0.52$ m from the junction, **(c)** in Pipe 3 at $x = 0.48$ m from the junction and **(d)** in Pipe 4 at $x = 0.43$ m from the junction.

the pressure waves and the junction in a satisfactory manner. Another important feature of the present approach is that no iterative method is required.

4. Conclusion and perspective

A numerical method for solving unsteady compressible non-equilibrium two-phase flows in networks of flexible pipelines is proposed. The compressible two-pressure two-fluid Baer-Nunziato model is here considered for compressible two-phase flow modeling. A Finite-Volume method using the Arbitrary Lagrangian-Eulerian formulation is used for the resolution of the Baer-Nunziato equations. The numerical coupling of several 1-D pipes converging into a junction is also addressed here. The approach approximates the junction as a multi-dimensional cell exchanging mass, momentum and energy with its adjacent pipes in the manner of [1]. As a consequence, no iterative procedure is used for this treatment of the junction problem. The same method is also applied to take into account the abrupt change of duct cross-sections. The present numerical approach is then assessed on several 1-D Riemann problems in both "subsonic" and "supersonic" configurations, shock-tubes and other transient flow problems involving abrupt change of area or junction of branched pipes. Some comparisons with experiments such as water-hammer with vapor cavity formation and collapse and pressure wave in a 3-pipe and 4-pipe network are also given showing the accuracy, robustness, generality and efficiency of the proposed numerical method.

The numerical scheme used in the present paper is only first-order accurate. Second-order accurate extension as the one proposed in [36] must be considered in the future to improve accuracy of the present methods. Furthermore, investigations may also concern the dynamic fluid-structure interaction which is necessary to estimate the mechanical consequences of pipeline systems subject to strong hydrodynamic loads. For example, the FSI junction coupling has to be considered at movable pipe ends, bends, valves and other places where strong forces between the pipe and the liquid exist. For this purpose, the Baer-Nunziato model has to be coupled with beam finite elements describing the behavior of the pipes in the manner of [1]. In addition, in certain situations, strong pressure waves can be generated by the direct contact condensation between hot vapor and cold water leading to the so-called condensation-induced water-hammer. For this dangerous phenomena, the interphase heat and mass transfer should also be taken into account as in [6, 43, 26]. Research of these issues is ongoing.

Acknowledgements

This work has been achieved within the framework of the "FAST" project of the EDF/CEA/Framatome tripartite institute. RAB acknowledges the U.S. DOE for support of research at the INL under contract DE-AC07-05ID14517. Computational facilities were provided by EDF. Numerical simulations have been performed with the *Europlexus* software.

References

[1] F. Daude, P. Galon, A Finite-Volume approach for compressible single- and two-phase flows in flexible pipelines with fluid-structure interaction, J. Comput. Phys. 362 (C) (2018) 375–408.
[2] N. Andrianov, G. Warnecke, On the solution to the Riemann problem for the compressible flow in a duct, SIAM J. Appl. Math. 64 (3) (2004) 878–901.
[3] D. Kröner, M.-D. Thanh, Numerical solution to compressible flows in a nozzle with variable cross-section, SIAM J. Numer. Anal. 43 (2) (2006) 796–824.
[4] S. Clain, D. Rochette, First- and second-order finite volume methods for the one-dimensional nonconservative Euler system, J. Comput. Phys. 228 (22) (2009) 8214–8248.
[5] D. Rochette, S. Clain, W. Bussière, Unsteady compressible flow in ducts with varying cross-section: Comparison between the nonconservative Euler system and the axisymmetric flow model, Comput. Fluids 53 (2012) 53–78.
[6] R. A. Berry, R. Saurel, O. Le Métayer, The discrete equation method (DEM) for fully compressible, two-phase flows in ducts of spatially varying cross-section, Nuclear Eng. Design 240 (11) (2010) 3797–3818.
[7] V. L. Streeter, E. B. Wylie, Hydraulic Transients, McGraw-Hill, New-York, 1967.
[8] A. Osiadacz, Simulation of transient gas flows in networks, Int. J. Numer. Meth. Fluids 4 (1) (1984) 13–24.
[9] M. K. Banda, M. Herty, A. Klar, Gas flow in pipeline networks, Netw. Heterog. Media 1 (2006) 41–46.
[10] R. A. Berry, L. Zou, R. C. Johns, R. C. Martineau, D. Andrs, H. Zhang, J. E. Hansel, RELAP-7 Progress Report: A Mathematical Model for 1-D Compressible, Single-Phase Flow Through a Branching Junction, Tech. Rep. INL/EXT-17-42938, Idaho National Laboratory (2017).

[11] R. M. Colombo, M. Gravello, A well-posed Riemann problem for the p-system at a junction, Netw. Heterog. Media 1 (2006) 495–511.
[12] G. A. Reigstad, T. Flåtten, Numerical investigation of network models for isothermal junction flow, in: Numerical Mathematics and Advanced Applications-ENUMATH 2013, Springer, 2015, pp. 667–675.
[13] G. A. Reigstad, Existence and uniqueness of solutions to the generalized Riemann problem for isentropic flow, SIAM J. Appl. Math. 75 (2) (2015) 679–702.
[14] C. Contarino, E. F. Toro, G. I. Montecinos, R. Borsche, J. Kall, Junction-Generalized Riemann Problem for stiff hyperbolic balance laws in networks: An implicit solver and ADER schemes, J. Comput. Phys. 315 (2016) 409–433.
[15] J. Gale, I. Tiselj, Water hammer in elastic pipes, International Conference on Nuclear Energy for New Europe '02, Kranjska Gora, Slovenia, Sept. 9-12, 2002.
[16] M. S. Ghidaoui, M. Zhao, D. A. McInnis, D. H. Axworthy, A review of water hammer theory and practice, ASME Appl. Mech. Rev. 58 (1) (2005) 49–76.
[17] M. Dumbser, U. Iben, M. Ioriatti, An efficient semi-implicit finite volume method for axially symmetric compressible flows in compliant tubes, Appl. Num. Math. 89 (2015) 24–44.
[18] J. Leibinger, M. Dumbser, U. Iben, I. Wayand, A path-conservative Osher-type scheme for axially symmetric compressible flows in flexible visco-elastic tubes, Appl. Num. Math. 105 (2016) 47–63.
[19] G. Bertaglia, M. Ioriatti, A. Valiani, M. Dumbser, V. Caleffi, Numerical methods for hydraulic transients in visco-elastic pipes, J. Fluids Struct. 81 (2018) 230–254.
[20] M. J. Castro, P. G. Le Floch, M. L. Muñoz Ruiz, C. Parés, Why many theories of shock waves are necessary: Convergence error in formally path-consistent schemes, J. Comput. Phys. 227 (17) (2008) 8107–8129.
[21] R. Abgrall, S. Karni, A comment on the computation of non-conservative products, J. Comput. Phys. 229 (8) (2010) 2759–2763.
[22] S. W. Hong, C. Kim, A new finite volume method on junction coupling and boundary treatment for flow network system analyses, Int. J. Numer. Meth. Fluids 65 (6) (2011) 707–742.
[23] A. Bermúdez, X. López, M. E. Vázquez-Cendón, Treating network junctions in finite volume solution of transient gas flow models, J. Comput. Phys. 344 (2017) 187–209.
[24] F. Daude, A. S. Tijsseling, P. Galon, Numerical investigations of water-hammer with column-separation induced by vaporous cavitation using a one-dimensional Finite-Volume approach, J. Fluids Struct. 83 (2018) 91–118.
[25] M. Dumbser, U. Iben, C.-D. Munz, Efficient implementation of high order unstructured WENO schemes for cavitating flows, Comput. Fluids 86 (2013) 141–168.
[26] H. Lochon, F. Daude, P. Galon, J.-M. Hérard, Computation of fast depressurization of water using a two-fluid model: Revisiting Bilicki modelling of mass transfer, Comput. Fluids 156 (2017) 162–174.
[27] R. A. Berry, L. Zou, H. Zhao, D. Andrs, J. Peterson, H. Zhang, R. C. Martineau, RELAP-7: Demonstrating Seven-Equation Two-Phase Flow Simulation in a Single-Pipe, Two-Phase Reactor Core and Steam Separator/Dryer, Tech. Rep. INL/EXT-13-28750, Idaho National Laboratory (2013).
[28] R. A. Berry, L. Zou, H. Zhao, H. Zhang, J. Peterson, R. C. Martineau, S. Y. Kadioglu, D. Andrs, RELAP-7 Theory Manual, Tech. Rep. INL/EXT-14-31366 (Revision 3), Idaho National Laboratory (2018).
[29] D. A. Drew, S. L. Passman, Theory of multicomponent fluids, Springer, New-York, 1998.
[30] M. Ishii, T. Hibiki, Thermo-Fluid Dynamics of Two-Phase Flow, Springer, New-York, 2006.
[31] R. A. Berry, Notes on Well-Posed, Ensemble Average Conservation Equations for Multiphase, Multi-Component, and Multi-Material Flows, Tech. Rep. INL/EXT-05-00516-modified, Idaho National Laboratory (2005).
[32] P. Embid, M. R. Baer, Mathematical analysis of a two-phase continuum mixture theory, Cont. Mech. Thermodyn. 4 (1992) 279–312.
[33] R. Saurel, R. Abgrall, A Multiphase Godunov Method for Compressible Multifluid and Multiphase Flows, J. Comput. Phys. 150 (2) (1999) 425–467.
[34] T. Gallouët, J.-M. Hérard, N. Seguin, Numerical modeling of two-phase flows using the two-fluid two-pressure approach, Math. Models Methods Appl. Sci. 14 (5) (2004) 663–700.
[35] N. Andrianov, G. Warnecke, The Riemann problem for the Baer-Nunziato two-phase flow model, J. Comput. Phys. 195 (2) (2004) 434–464.
[36] D. W. Schwendeman, C. W. Wahle, A. K. Kapila, The Riemann problem and a high-resolution Godunov method for a model of compressible two-phase flow, J. Comput. Phys. 212 (2) (2006) 490–526.
[37] S. A. Tokareva, E. F. Toro, HLLC-type Riemann solver for the Baer-Nunziato equations of compressible two-phase flow, J. Comput. Phys. 229 (10) (2010) 3573–3604.
[38] M. Dumbser, E. F. Toro, A simple extension of the Osher Riemann solver to non-conservative hyperbolic systems, J. Scientific Comp. 48 (2011) 70–88.
[39] F. Daude, P. Galon, On the computation of the Baer-Nunziato model using ALE formulation with HLL- and HLLC-type solvers towards fluid-structure interactions, J. Comput. Phys. 304 (2016) 189–230.
[40] H. Lochon, F. Daude, P. Galon, J.-M. Hérard, HLLC-type Riemann solver with approximated two-phase contact for the computation of the Baer-Nunziato two-fluid model, J. Comput. Phys. 326 (2016) 733–762.
[41] M. R. Baer, J. W. Nunziato, A two-phase mixture theory for the deflagration-to-detonation transition (ddt) in reactive granular materials, Int. J. Multiphase Flow 12 (6) (1986) 861–889.
[42] F. Coquel, T. Gallouët, J.-M. Hérard, N. Seguin, Closure laws for a two-fluid two-pressure model, C.R. Acad. Sci. Paris 334, Série I (10) (2002) 927–932.
[43] H. Lochon, F. Daude, P. Galon, J.-M. Hérard, Comparison of two-fluid models on steam-water transients, ESAIM Math. Model. Numer. Anal 50 (6) (2016) 1631–1657.
[44] C. Farhat, P. Geuzaine, C. Grandmont, The discrete geometric conservation law and the nonlinear stability of ALE schemes for the solution of flow problems on moving grids, J. Comput. Phys. 174 (2) (2001) 669–694.
[45] H. Luo, J. D. Baum, R. Lohner, On the computation of multi-material flows using ALE formulation, J. Comput. Phys. 194 (1) (2004) 304–328.
[46] F. Daude, P. Galon, Z. Gao, E. Blaud, Numerical experiments using a HLLC-type scheme with ALE formulation for compressible two-phase

flows five-equation models with phase transition, Comput. Fluids 94 (1) (2014) 112–138.
[47] F. Bellamoli, L. O. Müller, E. F. Toro, A numerical method for junctions in networks of shallow-water channels, Appl. Math. Comput. 337 (2018) 190–213.
[48] F. Bellamoli, Computational methods for coupling 1D and 2D channel geometries for the shallow water equations, Master's thesis, Università degli studi di Trento (2012).
[49] E. B. Wylie, V. L. Streeter, L. Suo, Fluid Transients in Systems, Prentice Hall, Englewood Cliffs, NJ, 1993.
[50] M. H. Chaudhry, Applied Hydraulic Transients, 3d edition, Springer, 2014.
[51] A. Bergant, A. R. Simpson, A. S. Tijsseling, Water hammer with column separation: A historical review, J. Fluids Struct. 22 (2) (2006) 135–171.
[52] D. J. Korteweg, Ueber die Fortplanzungsgeschwindigkeit des Schalles in Elastischen Röhren (On the velocity of propagation of sound in elastic pipes), Ann. Phys. Chemie 5 (1878) 525–542, (in German).
[53] L. Allievi, Teoria del colpo d'ariete, Atti del Collegio degli Ingegneri ed Architetti Italiani, Milan, Italy (in Italian), 1913, (English translation by E. E. Halmos 1925, *The theory of waterhammer*, Trans. ASME).
[54] A. S. Tijsseling, Water hammer with fluid-structure interaction in thick-walled pipes, Comput. Struct. 85 (2007) 844–851.
[55] Joint Research Centre (JRC), Commissariat à l'énergie atomique et aux énergies alternatives (CEA), *Europlexus* user's manual, http://europlexus.jrc.ec.europa.eu/ (2018).
[56] M. Dumbser, W. Boscheri, High-order unstructured Lagrangian one-step WENO finite volume schemes for non-conservative hyperbolic systems: Applications to compressible multi-phase flows, Comput. Fluids 86 (2013) 405–432.
[57] M. Dumbser, A. Hidalgo, O. Zanotti, High order space-time adaptive ADER-WENO finite volume schemes for non-conservative hyperbolic systems, Comput. Methods Appl. Mech. Engrg. 268 (24-25) (2014) 359–387.
[58] M.-D. Thanh, D. Kröner, C. Chalons, A robust numerical method for approximating solutions of a model of two-phase flows and its properties, Appl. Math. Comput. 219 (7) (2012) 320–344.
[59] S. Brown, S. Martynov, H. Mahgerefteh, Simulation of two-phase flow through ducts with discontinuous cross-section, Comput. Fluids 120 (2015) 46–56.
[60] A. R. Simpson, Large water hammer pressures due to column separation in sloping pipes (transient cavitation), Ph.D. thesis, The University of Michigan (1986).
[61] A. R. Simpson, E. B. Wylie, Large water-hammer pressures for column separation in pipelines, ASCE J. Hydraul. Engng. 117 (10) (1991) 1310–1316.
[62] I. Tiselj, A. Horvat, J. Gale, Numerical scheme for the WAHA Code, Multiph. Sci. Technol. 20 (3–4) (2008) 323–354.
[63] I. Tiselj, A. Horvat, G. Cerne, J. Gale, I. Parzer, B. Mavko, M. Giot, J.-M. Seynhaeve, B. Kucienska, H. Lemonnier, WAHA3 code manual, Final report of the WAHALoads project, Tech. Rep. FIKS-CT-2000-00106, EU 6th program (2004).
[64] L. Haar, J. S. Gallangher, G. S. Kell, NBS/NRC Steam Tables: Thermodynamic and Transport Properties and Computer Programs for Vapor and Liquid States of Water in SI Units, Hemisphere Publishing Co., 1984.
[65] M. J. P. William-Louis, A. Ould-El-Hadrami, C. Tournier, On the calculation of unsteady compressible flow through an N-branch junction, Proc. Instn. Mech. Engrs. 212 (1998) 49–56.
[66] J.-M. Hérard, O. Hurisse, A fractional step method to compute a class of compressible gas-liquid flows, Comput. Fluids 55 (2012) 57–69.
[67] S. Gavrilyuk, The structure of pressure relaxation terms: one-velocity case, Tech. Rep. H-I83-2014-00276-EN, EDF R&D (2014).

Appendix A. Pressure and velocity relaxations

The Baer-Nunziato model with interphase drag and pressure relaxation can be written as:

$$\begin{cases} \partial_t(\alpha_1 A) & & +u_I A\partial_x\alpha_1 & = & \alpha_1\partial_t A & +AK_p(p_1-p_2) & \\ \partial_t(\alpha_k\rho_k A) & +\partial_x(\alpha_k\rho_k u_k A) & & = & 0 & & \\ \partial_t(\alpha_k\rho_k u_k A) & +\partial_x\left(\alpha_k\rho_k u_k^2 A+\alpha_k p_k A\right) & -p_I A\partial_x\alpha_k & = & \alpha_k p_k\partial_x A & & +AK_u(u_{k'}-u_k) \\ \partial_t(\alpha_k\rho_k e_k A) & +\partial_x(\alpha_k\rho_k e_k u_k A+\alpha_k p_k u_k A) & -p_I u_I A\partial_x\alpha_k & = & -\alpha_k p_k\partial_t A & -Ap_I K_p(p_k-p_{k'}) & +AK_u u_I^*(u_{k'}-u_k) \end{cases}$$

where $k=1,2$, $k'=1,2$ $(k'\neq k)$, $u_I=u_2$ and $p_I=p_1$.

The velocity u_I^* is given by: $u_I^*=(u_1+u_2)/2$. The scalars K_p and K_u associated to the pressure and velocity relaxation, respectively, are positive functions given by [66]:

$$K_p=\frac{1}{\tau_p}\frac{\alpha_1\alpha_2}{|p_1|+|p_2|} \quad \text{and} \quad K_u=\frac{1}{\tau_u}\frac{\alpha_1\rho_1\alpha_2\rho_2}{\alpha_1\rho_1+\alpha_2\rho_2}$$

with τ_p and τ_u the relaxation time scales of pressure and velocity, respectively. Based on [67], the pressure relaxation time scale τ_p is evaluated using the Rayleigh-Plesset equation, which considers the evolution of a bubble in an infinite

medium. In addition, the evaluation of the velocity relaxation time scale τ_u is based on the drag equation for the behavior of a bubble in an infinite medium. More details are given in [43, 26].

The Baer-Nunziato model with interphase drag and pressure relaxation is then approximated using a fractional step approach as in [43] where more details concerning the numerical approximation of the pressure and velocity relaxation terms can be found.